



1 **Low CO₂ evasion rate from the mangrove surrounding waters of Sundarban**

2 Anirban Akhand¹, Abhra Chanda², Kenta Watanabe¹, Sourav Das², Tatsuki Tokoro¹, Kunal

3 Chakraborty³, Sugata Hazra², Tomohiro Kuwae¹

4 ¹Coastal and Estuarine Environment Research Group, Port and Airport Research Institute, 3-1-1

5 Nagase, Yokosuka 239-0826, Japan.

6

7 ²School of Oceanographic Studies, Jadavpur University, 188, Raja S. C. Mullick Road, Kolkata

8 700 032, West Bengal, India.

9

10 ³Indian National Centre for Ocean Information Services, Ocean Valley, Pragathi Nagar (BO),

11 Nizampet (SO), Hyderabad 500 090, India

12

13 Running Head: Low CO₂ evasion from mangrove water

14

15

16

17

18

19

20

21

22

23



24

25 **Abstract**

26 Globally, water bodies adjacent to mangroves are considered sources of atmospheric CO₂. We
27 directly measured the partial pressure of CO₂ in water, pCO₂(water), and other related
28 biogeochemical parameters with very high (1-min) temporal resolution at Dhanchi Island in
29 India's Sundarbans during the post-monsoon season. We used elemental, stable isotopic, and
30 optical signatures to investigate the sources of dissolved inorganic carbon (DIC) and organic
31 matter (OM) in these waters. Diel mean pCO₂(water) was marginally oversaturated in creeks
32 (efflux, $69 \pm 180 \mu\text{mol m}^{-2} \text{h}^{-1}$) and undersaturated along the island boundary and in the main
33 river (influx, -17 ± 53 and $-31 \pm 73 \mu\text{mol m}^{-2} \text{h}^{-1}$, respectively) compared to the atmospheric
34 CO₂ concentration. The possibility in earlier studies of over- or underestimating the CO₂ flux
35 because of an inability to capture tidal minima and maxima was minimized in the present study,
36 which confirmed that the waters surrounding mangroves in this region can act as a sink or a very
37 weak source of atmospheric CO₂. $\delta^{13}\text{C}$ values for DIC suggest a mixed DIC source, and a three-
38 end-member stable isotope mixing model and optical signatures of OM suggest negligible
39 riverine contribution of freshwater to OM. We conclude that the CO₂ sink or weak source
40 character was due to a reduced input of riverine freshwater [which usually has high pCO₂(water)]
41 and the predominance of pCO₂-lean water from the coastal sea, which eventually increases the
42 buffering capacity of the water as evidenced by the Revelle factor. Up-scaling the CO₂ flux data
43 for all seasons and the entire estuary, we propose that the CO₂ evasion rate observed in this study
44 is much lower than the recently estimated world average. Mangrove areas having such low
45 emissions should be given due emphasis when up-scaling the global mangrove carbon budget
46 from regional observations.



47

48 Keywords: Air–water CO₂ flux; estuary; mangrove-associated water; net CO₂ sink; pCO₂(water);
49 stable isotope

50

51 **1. Introduction**

52 According to the Fifth Assessment Report (AR5) of the Intergovernmental Panel on
53 Climate Change (IPCC) (IPCC, 2014), greenhouse gas emissions increased at a rate of 2.2% per
54 year during the last decade (2000–2010) and the emission rate reached 49 ± 4.5 Pg CO₂-
55 equivalents y⁻¹ in 2010. The carbon stocks within several coastal ecosystems (mangroves, tidal
56 marshes, seagrass beds), collectively referred to as “blue carbon”, have drawn attention in this
57 regard (Donato et al., 2011; McLeod et al., 2011; Pendleton et al., 2012), and initiatives to
58 characterize the functioning and long-term future of these blue-carbon ecosystems have also
59 begun (Macreadie et al., 2019). All of these ecosystems are known to be carbon sinks;
60 mangroves, however, deserve special mention owing to their large soil organic pool and their
61 being an active deposition centre for both autochthonous and allochthonous organic matter
62 (Breithaupt et al., 2012; Sanders et al., 2016a, 2016b).

63 Globally, mangroves reportedly have an estimated mean net primary production of $218 \pm$
64 72 Tg C y⁻¹ (Bouillon et al., 2008; Fuentes and Barr, 2015). Moreover, the combined carbon (C)
65 stock in mangroves (above ground and live belowground; 956 Mg C ha⁻¹) is much higher than
66 that in other carbon rich ecosystems such as salt marshes (593 Mg C ha⁻¹), seagrasses (142 Mg C
67 ha⁻¹), peatland (408 Mg C ha⁻¹), or even rain forests (241 Mg C ha⁻¹) (Alongi, 2014; Donato et
68 al., 2011; Twilley et al., 1992). Despite covering only 0.1% of the earth’s total land area
69 (Jennerjahn and Ittekkot, 2002), 0.7% of tropical forests globally (Giri et al., 2011), and 0.5% of



70 the global coastal ocean (Rosentreter et al., 2018), mangroves are one of the most productive
71 ecosystems in the world, with high carbon-sequestration potential.

72 Although mangrove ecosystems as a whole are net sinks for CO₂, the waters adjacent to
73 mangroves (as well as sediments) emit substantial amounts of CO₂, because they have substantial
74 organic carbon loading, which is mainly attributed to mangrove biomass, terrestrial detritus,
75 microphytobenthos, land-driven allochthonous nutrients, and phytoplankton (Borges et al., 2005,
76 2018; Borges and Abril, 2011; Bouillon and Boschker, 2006; Kristensen et al., 2008; Lekphet et
77 al., 2005). In contrast to processes in other forests, tidal flow allows mangroves to exchange both
78 inorganic and organic solutes and particulates with adjacent water bodies (Adame and Lovelock,
79 2011). Several studies have attributed the high CO₂ emissions from the waters surrounding
80 mangroves to the efficient exchange and mixing of surface water with pore water through tidal
81 pumping, leading to enrichment of the partial pressure of CO₂ in water [pCO₂(water)] and
82 dissolved inorganic carbon (DIC), as well as metabolic activity in sediments (Bouillon et al.,
83 2007b; Gleeson et al., 2013; Li et al., 2009; Maher et al., 2013; Robinson et al., 2007; Santos et
84 al., 2012; Sippo et al., 2016).

85 Processes such as the mineralization of dissolved organic carbon (DOC) and particulate
86 organic carbon (POC) lead to additional DIC in water bodies adjacent to mangroves (Gattuso et
87 al., 1998; Maher et al., 2013, 2015). The mineralization of organic carbon in mangrove
88 sediments is facilitated through several pathways such as sulfate reduction, iron reduction,
89 aerobic respiration, and carbonate dissolution (Borges et al., 2003; Kristensen and Alongi, 2006;
90 Krumins et al., 2013).



91 Although the mangroves surrounding waters usually act as a source of CO₂, there are still
92 uncertainties with respect to the global budget of these emissions. In their global estimates,
93 studies carried out during the last decade mostly considered the total mangrove area of the globe
94 to be the total area of the water adjoining the mangroves (Borges et al., 2003; Koné and Borges,
95 2008), which is certainly not the actual case (Sippo et al., 2016). Moreover, these studies never
96 reported negative fluxes (i.e., the water surrounding mangroves acting as a sink for CO₂).
97 However, some recent measurements in mangroves surrounding waters show negative fluxes in
98 some regions, and at certain times of the year CO₂ fluxes in mangrove waters can be negative as
99 well (Biswas et al., 2004; Akhand et al., 2013b, 2016). In addition, Call et al. (2015) recently
100 observed very low effluxes (almost zero) in a sub-tropical mangrove ecosystem in Australia. In
101 this regard, Rosentreter et al. (2018) emphasized the temporal resolution of sampling, which can
102 lead to considerable uncertainty. They argued that data acquisition at hourly or greater intervals
103 often misses the tidal maxima and minima, and deducing the mean CO₂ flux from such data
104 might lead to under- or overestimation of fluxes.

105 At present, all rivers in the Indian part of the Sundarbans except for the Hooghly and its
106 distributary the Muriganga – namely the Saptamukhi, Thakuran, Matla, Gosaba, and Bidya rivers
107 – have lost their connections with the main flow of the River Ganga because of siltation in the
108 upper reaches; their estuarine character is now maintained only by monsoonal runoff (Cole and
109 Vaidyaraman, 1966; Sarkar et al., 2004). Thus, the central part of the Sundarbans lacks riverine
110 freshwater input (Chakrabarti, 1998; Mitra et al., 2009).

111 In the last decade, the air–water CO₂ flux has been well studied in the Indian section of
112 the Sundarbans from the perspective of spatial variability (Akhand et al., 2013b, 2016; Dutta et
113 al., 2019) and seasonal variability (Biswas et al., 2004; Akhand et al., 2016). Hence, in this study



114 we do not emphasize these two aspects. Rather, we focus on a particular site and season
115 previously reported as being a maximum sink or reduced source of CO₂ (Biswas et al., 2004;
116 Akhand et al., 2016) in order to carry out a thorough and comprehensive investigation into the
117 reasons for such a sink or reduced source. However, as there is no well-defined demarcation of
118 “mangroves surrounding waters”, we set up sampling stations in three types of water bodies
119 around the mangroves in the study area, namely creeks, island boundaries, and the main river,
120 which are usually considered as the waters surrounding mangroves. These stations are mostly in
121 the sub-tidal zone, although the island boundary stations were chosen as close to the intertidal
122 zone as possible.

123 We hypothesized that despite being an ecosystem of mangroves surrounded by water, the
124 CO₂ sink or weak source character of the Indian Sundarbans is mainly caused by the negligible
125 riverine freshwater contribution of carbon species. To examine this hypothesis, we used
126 automated data collection to obtain high-temporal-resolution data for pCO₂(water) and other
127 related biogeochemical parameters. To our knowledge, this is the first time in the Sundarban that
128 this type of data has been collected at this temporal resolution. In addition, we used elemental,
129 stable isotopic, and optical signatures to quantify the carbon load in the surface water and to
130 identify the carbon sources at our site, which identified as a CO₂ sink or weak source in previous
131 studies. Finally, we up-scaled our CO₂ flux data for all seasons and for the whole estuary and
132 then compared them with the global average data. Out of the many estuaries that flow through
133 Sundarbans, we considered the Matla Estuary for up-scaling, as this estuary flows through the
134 central part of Indian Sundarban and flows for a long distance covering almost the entire north-
135 south extent of Sundarbans. Moreover, this estuary has been exhaustively studied in the recent
136 past from the perspective of air–water CO₂ flux. Though the present study site is located near the



137 Thakuran Estuary, we assume that since Matla and Thakuran are adjacent estuaries, there is no
138 significant difference in their biogeochemical characteristics.

139 Our objectives were (a) to reduce the uncertainty of flux estimation by direct and
140 continuous measurement of $p\text{CO}_2(\text{water})$ and related biogeochemical parameters, (b) to examine
141 the role of mangrove-derived carbon (DIC, DOC and POC) in the air–water CO_2 flux, (c) to
142 estimate the net ecosystem productivity and calcification rates in the waters around the
143 mangroves by using high-temporal-resolution biogeochemical data, and finally (d) to identify an
144 understandable reason behind the transient sink character of this region despite its being
145 surrounded by dense mangrove vegetation.

146

147 **2. Materials and methods**

148 **2.1 Study area**

149 The Sundarbans, a UNESCO world heritage site, is the world's largest mangrove forest.
150 It is situated in the lower stretch of Ganges-Brahmaputra-Meghna (GBM) Delta and extends into
151 the countries of both India (40%) and Bangladesh (60%) and faces the Bay of Bengal (BoB) to
152 the south. The present study was carried out in the Indian part of the Sundarbans, which
153 comprises an area of $10,200 \text{ km}^2$ out of which 4200 km^2 is demarcated as reserve forest (Ray et
154 al., 2015). Sampling was conducted in a north–south channel approximately 9 km long (width
155 varying between 0.70 and 0.85 km) to the west of Dhanchi Island, at the edge of the island, and
156 in two very narrow (20 m wide) creeks flowing through the island (Fig. 1). For details about the
157 study area see Section S1 in the supplementary material. Dhanchi Island covers an area of about



158 33 km², and its southern tip ends at the BoB. To the east of the island flows the Thankuran River
159 (7 km wide).

160 **2.2 Sampling strategy**

161 The sampling stations were selected in order to understand, characterize and differentiate
162 the carbon dynamics in three types of waters: waters likely to be strongly influenced by
163 mangroves, waters under the combined influence of both mangrove-driven pore water and
164 seawater coming through the channel, and waters minimally influenced by mangroves (Fig. 1).
165 We selected eight sampling locations (all subtidal) in the westward channel adjoining Dhanchi
166 Island and in two creeks connected to that channel. One of the creek stations was 9 km north of
167 the BoB coast (hereafter referred to as C1) and the other 5 km north (C2). We selected three
168 locations covering the latitudinal extent of the north–south channel very close to the edge of the
169 Dhanchi Island boundary (10 m from the island’s landmass), designated as IB1 (9 km from the
170 BoB), IB2 (5 km), and IB3 (1 km). The remaining three stations were selected at the same
171 latitudes as IB1, IB2, and IB3, respectively, only in the middle of the channel, hereafter referred
172 to as MR1 (9 km from the BoB), MR2 (5 km), and MR3 (1 km). Collectively, the abbreviations
173 “C”, “IB” and “MR” stand for creek, island boundary and mid-river stations, respectively.

174 **2.3 Sample collection**

175 Surface pCO₂(water), salinity, water temperature, dissolved oxygen, pH, and above-water
176 photosynthetic photon flux density were monitored with sensors (for details see section 2.4).
177 Water depth was recorded every hour by using a weighted line and a tape measure. Data for a 24
178 h diurnal cycle for all of these parameters were acquired at 1 min intervals at each of the eight
179 stations between 27 January and 6 February 2018. Surface water samples were collected at two



180 peak low and high tides during the diurnal cycles. In addition, surface water samples were
181 collected offshore (about 60 km off the coast in the BoB) from on-board a fishing trawler, and
182 from a station in Diamond Harbour (salinity approx. 0), which served as the marine end member
183 (MEM) and freshwater end member (FWEM), respectively. The samples were preserved as
184 described in the next paragraph and sent to the laboratory for analysis.

185 Samples for total alkalinity (TAlk) and DIC were collected into 250 mL Duran bottles
186 (SCHOTT AG, Mainz, Germany), filtered through glass-fibre filters (GF/F; Whatman,
187 Maidstone, Kent, UK) and poisoned with mercuric chloride (200 μ L saturated aqueous solution
188 per bottle) to prevent changes in TAlk and DIC due to biological activity. Samples for DOC and
189 optical analysis of chromophoric dissolved organic matter (CDOM) were filtered through 0.2 μ m
190 polytetrafluoroethylene (PTFE) filters (DISMIC-25HP; Advantec, Durham, NC, USA) into pre-
191 combusted (450 °C for 2 h) 100 mL glass vials. DOC samples were acidified with H₃PO₄ to a pH
192 of <2 and then frozen at –20 °C until analysis. CDOM samples were kept at 4 °C until analysis.
193 Samples for analysis of POC, particulate nitrogen (PN), and for stable isotope analysis ($\delta^{13}\text{C}_{\text{POC}}$
194 and $\delta^{15}\text{N}_{\text{PN}}$) were obtained by filtration (approx. 1–2 L) onto pre-combusted (450 °C for 2 h)
195 glass-fibre filters (GF/F; Whatman) and stored in the dark at –20 °C until analysis.

196 Mangrove leaves were collected to determine the stable isotope signatures ($\delta^{13}\text{C}_{\text{POC}}$ and
197 $\delta^{15}\text{N}_{\text{PN}}$) of the mangrove as an end member. Leaves of the dominant mangrove species of the
198 Indian Sundarbans (Gopal and Chauhan, 2006) – *Avicennia marina*, *Bruguiera gymnorrhiza*,
199 *Excoecaria agallocha*, and *Phoenix paludosa* – were collected and stored at –20 °C until
200 analysis.

201 **2.4 Analytical protocol**



202 TAlk and DIC concentrations were determined on a batch-sample analyser (ATT-05;
203 Kimoto Electric Co., Ltd., Osaka, Japan) implementing the Gran Plot method (Dickson et al.,
204 2007). The accuracy of TAlk and DIC was $3 \mu\text{mol kg}^{-1}$ water and $4 \mu\text{mol kg}^{-1}$ water,
205 respectively, which was confirmed by triplicate measurements of the certified reference material
206 (CRM) for TAlk and DIC (Kanso Company Ltd., Japan). The $\text{pCO}_2(\text{water})$ was measured with a
207 CO_2 analyser (Non Dispersive Infrared Sensor) through an equilibrator system (CO_2 -09, Kimoto
208 Electric Co., Ltd.) (Kayanne et al., 1995; Tokoro et al., 2014) using a gas-permeable membrane
209 (Saito et al., 1995). The instrument was calibrated every day at the beginning of the
210 measurements using pure N_2 gas (0 ppm) and span gas (600 ppm CO_2 gas with a N_2 base;
211 Chemtron Science Laboratories, India). pH was measured with a sensor (SP-11; Kimoto
212 Electric). We collected about 10 water samples from different stations and at different times
213 during sampling and calibrated the pH sensor. The pH of the water samples was calculated from
214 the measured TAlk and DIC using equilibrium calculations. The pH was finally corrected by the
215 calibration line from the least-squares regression between the raw sensor data (electromotive
216 force of the pH electrode) and the difference between the calculated pH and in situ pH, which are
217 proportional, as indicated by the Nernst equation. The precision of pH and pCO_2 was estimated
218 to be 0.002 and $2 \mu\text{atm}$, respectively.

219 Salinity and temperature were measured with a CT-sensor (INFINITY-CT;
220 JFE Advantech, Nishinomiya, Japan). Dissolved oxygen (DO) concentration was measured at
221 hourly intervals with a portable DO meter (FiveGo Series; Mettler Toledo, Germany). DOC
222 concentration was determined via high-temperature catalytic oxidation with a TOC analyser
223 (TOC5000A; Shimadzu, Kyoto, Japan). DOM absorbance spectra were recorded from 250 to
224 700 nm at 1 nm increments using a UV-visible spectrometer (UV-2450; Shimadzu) fitted with a



225 1 cm quartz flow-cell and referenced to ultrapure water (Milli-Q water; Millipore, Billerica, MA,
226 USA). The absorbance values at each wavelength were transformed into absorption coefficients
227 (a_{CDOM}) by using the following equation:

228

$$229 \quad a_{\text{CDOM}(\lambda)} = 2.303 \times A_{\text{CDOM}(\lambda)} (\text{m}^{-1}), \quad (1)$$

230

231 where A_{CDOM} is the absorbance value per metre. The absorption value at 375 nm, $a_{\text{CDOM}(375)}$, was
232 chosen to quantify CDOM because this wavelength has been commonly used in previous studies
233 to measure DOC absorbance. We also measured $a_{\text{CDOM}(254)}$ as a metric of the aromaticity of the
234 DOM. We calculated specific UV absorption at 254 nm (SUVA_{254} , $\text{L mg}^{-1} \text{m}^{-1}$) as follows:

235

$$236 \quad \text{SUVA}_{254} = A_{\text{CDOM}(254)} / [\text{DOC}], \quad (2)$$

237

238 where [DOC] denotes DOC concentration. Spectral slopes for the interval of 275–295 nm (S_{275-}
239 $295}$) were calculated by linear regression of the log-transformed a_{CDOM} spectra. Slopes are
240 reported as positive numbers to follow the mathematical convention of fitting to an exponential
241 decay.

242 Samples for analysis of POC and PN content and stable isotope signatures ($\delta^{13}\text{C}$ and
243 $\delta^{15}\text{N}$) were dried in an oven at 60 °C. To remove inorganic carbon, we acidified the samples with
244 1 N HCl and dried them again at 60 °C. POC and PN concentrations and stable isotope



245 signatures were measured with an isotope-ratio mass spectrometer (Delta Plus Advantage;
246 Thermo Electron, Bremen, Germany) coupled with an elemental analyser (Flash EA 1112;
247 Thermo Electron). Stable isotope ratios are expressed in δ notation as the deviation from
248 standards in parts per thousand (‰) according to the following equation:

249

$$250 \quad \delta_{13\text{C}}, \delta_{15\text{N}} = [R_{\text{sample}}/R_{\text{standard}} - 1] \times 10^3, \quad (3)$$

251

252 where R is $^{13}\text{C}/^{12}\text{C}$ or $^{15}\text{N}/^{14}\text{N}$. Vienna PeeDee Belemnite (VPDB) and atmospheric nitrogen
253 were used as the isotope standards for carbon and nitrogen, respectively. The analytical precision
254 of the Delta Plus Advantage mass-spectrometer system, based on the standard deviation of the
255 internal reference replicates, was $<0.2\text{‰}$ for both $\delta^{13}\text{C}$ and $\delta^{15}\text{N}$. The $\delta^{13}\text{C}_{\text{DIC}}$ was also measured
256 with the same isotope-ratio mass spectrometer following the method of Miyajima et al. (1995).

257 **2.5 Estimation of air–water CO₂ flux, net ecosystem production (NEP), and net ecosystem** 258 **calcification (NEC)**

259 The air–water CO₂ flux (F_{CO_2} , $\mu\text{mol CO}_2 \text{ m}^{-2} \text{ h}^{-1}$) was determined by the following
260 equation:

261

$$262 \quad F_{\text{CO}_2} = k \cdot K_0 \cdot \Delta f\text{CO}_2, \quad (4)$$

263



264 where k is the gas transfer velocity (cm h^{-1}), K_0 denotes the solubility coefficient of CO_2 (mol m^{-3}
265 atm^{-1}), and $\Delta f\text{CO}_2$ denotes the difference in fugacity (\approx partial pressure) of CO_2 between water
266 and air [$f\text{CO}_{2(\text{water})} - f\text{CO}_{2(\text{air})}$]. A positive F_{CO_2} value indicates CO_2 efflux from the water to the
267 atmosphere and vice versa. The parameter k was calculated according to formula of Ho et al.
268 (2011) based on wind speed. These formulae were selected for the present study as the estuarine
269 channels in the Indian part of the Sundarbans are much wider and with little to hinder free-
270 flowing wind compared to conditions in Hudson Bay observed by Ho et al. (2014). This formula
271 was obtained by deploying tracers for measuring the gas transfer velocity in the Hudson River:

272

$$273 \quad k = (a + 0.266 U_{10}^2) (\text{Sc}/600)^{-0.5}, \quad (5)$$

274

275 where U_{10} is the wind speed at 10 m height and a is a constant accounting for gas transfer from
276 bottom-shear-driven turbulence. Wind speed data were acquired by using a handheld
277 anemometer (AM 4201; Lutron Inc, Singapore.) and corrected for 10 m height (Kondo, 2000).
278 Sc is the Schmidt number of CO_2 as given by Wanninkhof (2014). K_0 is computed based on the
279 equation given by Weiss (1974).

280 Net ecosystem production (NEP) and net ecosystem calcification (NEC) were computed
281 from estimated DIC and TAlk (for details see Section S2 in the supplementary material).

282 **2.6 Data analysis**

283 To estimate the biological or physicochemical formation, transformation, and
284 consumption of carbon species in the water column, we calculated the difference between the



285 observed concentration of an element (X) and its concentration predicted by conservative mixing
286 (X_{mix}) as ΔX for each station: $\Delta X = X - X_{\text{mix}}$. The ΔX concentrations were determined for TALK,
287 DIC, DOC, $\delta^{13}\text{C}_{\text{DIC}}$, $a_{\text{CDOM}(375)}$, $a_{\text{CDOM}(254)}$, SUVA_{254} , and $\text{S}_{275-295}$. Predicted conservative
288 concentrations (X_{mix}) were estimated by using a linear salinity mixing model for TALK, DIC,
289 DOC, $a_{\text{CDOM}(375)}$, and $a_{\text{CDOM}(254)}$. Predicted conservative mixing lines (nonlinear) for SUVA_{254}
290 and $\text{S}_{275-295}$ were drawn from the concentrations of previously mentioned parameters, whereas
291 X_{mix} of the $\delta^{13}\text{C}_{\text{DIC}}$ were adopted according to the formula proposed by Mook and Tan (1991).

292 The Hooghly River is the main “artery” (Ray et al., 2018a) and only possible source of
293 riverine freshwater for the Indian Sundarbans, and the adjacent sea is the BoB. For this reason,
294 the near-zero salinity regime of the Hooghly River and the northern BoB have been universally
295 used in previous works (Ray et al., 2015, 2018a; Ray and Shahraki, 2016; Dutta et al., 2019) as
296 freshwater and marine end-members, respectively, in their mixing models for the Indian part of
297 the Sundarbans. As in these previous studies, we defined the observed salinity at the Diamond
298 Harbour station (salinity approx. 0) as a proxy for the riverine freshwater end member (FWEM)
299 and that offshore in the BoB (approx. 60 km off the coast) as the marine end member (MEM).

300 The FWEM and MEM samples were collected in triplicate simultaneously during our
301 sampling in the Sundarbans. Our measured TALK ($1646 \mu\text{mol kg}^{-1}$) and DIC ($1476 \mu\text{mol kg}^{-1}$) of
302 the MEM is in agreement with the post-monsoon data of Akhand et al. (2012, 2013a). In
303 contrast, Goyet et al. (1999) reported TALK and total CO_2 of 2180 and $1852 \mu\text{mol kg}^{-1}$,
304 respectively, in the surface water of the BoB, although their study site was far offshore (i.e. at
305 around 10° N latitude). Also, TALK and DIC of the MEM (same site as the present study) were
306 higher during other seasons: TALK pre-monsoon, $1932 \mu\text{mol kg}^{-1}$; monsoon, $1879 \mu\text{mol kg}^{-1}$;
307 DIC pre-monsoon, $1744 \mu\text{mol kg}^{-1}$; monsoon, $1643 \mu\text{mol kg}^{-1}$; (unpublished data, Akhand et



308 al.). Hence, it is apparent that both TAlk and DIC are lower in the northern BoB than farther
309 offshore, and both decrease further during the post-monsoon season. The lower values might be
310 due to biogenic activity, as the post-monsoon season is when phytoplankton blooms form in this
311 region. However, published and unpublished data consistently show that the BoB is pCO₂-lean
312 and the TAlk:DIC ratio is >1.

313 We used the Bayesian isotopic modelling package Stable Isotope Analysis in R (SIAR)
314 (Parnell et al., 2010) to partition the proportional contributions of potential organic matter (OM)
315 sources to the bulk particulate organic matter (POM) based on their N/C, δ¹³C, and δ¹⁵N
316 signatures. The SIAR model works by determining the probability distributions of the sources
317 that contribute to the observed mixed signal while accounting for the uncertainty in the
318 signatures of the sources and isotopic fractionation. We assumed an isotopic fractionation of zero
319 and ran the model through 1 × 10⁶ iterations. For each potential source, we report the median and
320 95% credible interval (CI) of the estimated proportional contribution to the observed value. We
321 defined three sources – freshwater-derived OM, mangrove-plant-derived OM, and marine OM –
322 as end members for the isotopic and elemental mixing model.

323 To characterize the pathway of mineralization of organic matter in this study, TAlk and
324 DIC were both normalized with respect to salinity. We analysed the stoichiometric relationship
325 (the slope) between salinity-normalized TAlk (nTAlk) and salinity-normalized DIC (nDIC). DIC
326 was normalized according to the following equation (Friis et al., 2003):

327

$$328 \quad \text{nDIC} = \left\{ \left[\frac{\text{DIC}_{\text{meas}} - \text{DIC}_{s=0}}{S_{\text{meas}}} \right] \times S_{\text{mean}} \right\} + \text{DIC}_{s=0}, \quad (6)$$

329



330 where DIC_{meas} is the measured DIC, $DIC_{s=0}$ is the DIC of the FWEM (i.e. where salinity = 0),
331 S_{meas} is the measured salinity, and S_{mean} is the mean salinity, which is used for normalization
332 (25.0 for this study). TALK was also normalized using the same equation, replacing DIC_{meas} and
333 $DIC_{s=0}$ with $TALK_{meas}$ and $TALK_{s=0}$, respectively.

334 The Revelle factor indicates the resistance of the ocean surface layer to absorbing
335 atmospheric CO_2 . We used CO_2SYS software to estimate the Revelle factor from the measured
336 TALK and DIC at the eight C, IB, and MR stations and at the FWEM and MEM stations.

337

338 3. Results

339 3.1 Physicochemical setting

340 The average depths of the C, IB, and MR stations were 4, 3, and 6 m, respectively. The
341 salinity of the FWEM was almost zero (0.39), and the salinity of the MEM was 26.9. All of the
342 mean values, standard deviations, and ranges of physicochemical, stable isotopic, and carbonate-
343 chemistry parameters are in Table S1 (supplementary material). The photosynthetic photon flux
344 at the water surface varied between $770 \pm 517 \mu\text{mol m}^{-2} \text{s}^{-1}$ (mean \pm s.d.; $n = 1406$) and $834 \pm$
345 $550 \mu\text{mol m}^{-2} \text{s}^{-1}$ ($n = 1831$) (see Fig. S1 in the supplementary material for the diel variability).
346 Water temperature varied within the narrow range between $21.18 \pm 0.66 \text{ }^\circ\text{C}$ ($n = 2880$) and 21.79
347 $\pm 0.49 \text{ }^\circ\text{C}$ ($n = 4320$) (Fig. 2). The salinity also varied within a very narrow range. The salinities
348 were 25.37 ± 0.65 at C stations ($n = 2880$), 25.63 ± 0.46 at IB stations ($n = 4320$), and $25.62 \pm$
349 0.35 at MR stations ($n = 4320$). DO concentrations gradually and slightly increased from C (5.1
350 $\pm 0.2 \text{ mg L}^{-1}$; $n = 48$), to IB ($5.5 \pm 0.2 \text{ mg L}^{-1}$; $n = 72$) and MR stations ($5.9 \pm 0.2 \text{ mg L}^{-1}$; $n =$
351 72).



352 3.2 Carbonate-chemistry parameters

353 The maximum $p\text{CO}_2(\text{water})$ was at C ($470 \pm 162 \mu\text{atm}$, $n = 2880$), and decreased
354 gradually toward IB ($393 \pm 48 \mu\text{atm}$, $n = 4320$) and MR ($380 \pm 66 \mu\text{atm}$, $n = 4320$) (Fig. 2).
355 Similarly, pH increased from 8.023 ± 0.015 ($n = 1337$) at C to 8.032 ± 0.009 ($n = 720$) at IB
356 (Table S1). The pH at MR, however, was 8.030 ± 0.002 ($n = 1440$), which is almost same as that
357 at IB. Measured TAlk showed a similar trend: C ($2047 \pm 289 \mu\text{mol kg}^{-1}$; $n = 8$), IB (1936 ± 146
358 $\mu\text{mol kg}^{-1}$; $n = 11$) and MR ($1887 \pm 19 \mu\text{mol kg}^{-1}$; $n = 12$). The measured DIC data showed a
359 gradual decrease from C ($2219 \pm 244 \mu\text{mol kg}^{-1}$; $n = 8$), to IB ($2112 \pm 120 \mu\text{mol kg}^{-1}$; $n = 11$)
360 and MR ($2078 \pm 17 \mu\text{mol kg}^{-1}$; $n = 12$). The measured TAlk and DIC of the FWEM were 2977
361 and $2950 \mu\text{mol kg}^{-1}$, respectively. The measured TAlk and DIC of the MEM were much lower at
362 1647 and $1476 \mu\text{mol kg}^{-1}$, respectively).

363 We plotted all of the TAlk and DIC values from our sampling sites onto the same graph
364 along with the conservative mixing line (Fig. 3a and 3b). $\delta^{13}\text{C}$ of DIC varied over a wide range,
365 from -1.5‰ to -7.6‰ with a mean of $-2.4\text{‰} \pm 1.3\text{‰}$ ($n = 31$). The $\delta^{13}\text{C}$ values for DIC were $-$
366 6.6‰ and -1.2‰ in the FWEM and MEM, respectively. Most of the DIC $\delta^{13}\text{C}$ values from C
367 stations plotted below the conservative mixing line, whereas values from IB and MR stations
368 plotted in a mixed fashion (below, along, or above the conservative mixing line; Fig. 3i). The
369 mean Revelle factors for the C, IB, and MR stations were 12.8 ± 2.1 (range, 11.2–17.9, $n = 8$),
370 12.4 ± 1.4 (11.5–16.3, $n = 11$), and 11.8 ± 0.3 (11.5–12.6, $n = 12$), respectively. The Revelle
371 factors for the MEM and FWEM were 10.7 and 26.7, respectively.

372 3.3 Air–water CO_2 flux



373 All three sampling zones (i.e. C, IB, and MR) varied diurnally between acting as a sink or
374 source of atmospheric CO₂ (Fig. 2). The creeks acted as net sources of CO₂ with a mean flux of
375 $69 \pm 180 \mu\text{mol m}^{-2} \text{h}^{-1}$ ($n = 2880$) and a range of $104\text{--}887 \mu\text{mol m}^{-2} \text{h}^{-1}$. In contrast, the island
376 boundary and mid-river acted as net sinks for CO₂ with mean fluxes of $-17 \pm 53 \mu\text{mol m}^{-2} \text{h}^{-1}$ (n
377 $= 4320$) and $-31 \pm 73 \mu\text{mol m}^{-2} \text{h}^{-1}$ ($n = 4320$), respectively (Table S1). The flux ranged between
378 $-108 \mu\text{mol m}^{-2} \text{h}^{-1}$ and $225 \mu\text{mol m}^{-2} \text{h}^{-1}$ at IB, and between $-99 \mu\text{mol m}^{-2} \text{h}^{-1}$ and $251 \mu\text{mol m}^{-2}$
379 h^{-1} at MR. We observed a distinct switch from a net CO₂ source at the creek stations to a net sink
380 at the island boundary. Moreover, the magnitude of the sink increased from IB to MR.

381 **3.4 NEP and NEC**

382 The photosynthesis–irradiance curve-fitting with measured NEP and NEC yielded
383 statistically significant relationships only at C2 among the eight stations (Fig. 4). NEP and NEC
384 at C2 were $-239 \text{mmol m}^{-2} \text{d}^{-1}$ ($R^2 = 0.66$, $P < 0.0001$) and $-149 \text{mmol m}^{-2} \text{d}^{-1}$ ($R^2 = 0.66$, $P <$
385 0.0001) respectively.

386 **3.5 Organic matter input**

387 Most of the DOC values were higher than those predicted by conservative mixing (Fig.
388 3c). The changes in POC, PN, POC:PN, $\delta^{13}\text{C}_{\text{POC}}$, and $\delta^{15}\text{N}_{\text{PN}}$ with salinity are shown in Fig. 3d–
389 3h. The $\delta^{13}\text{C}$ of TOC of leaves from the four dominant mangrove species was $-29.0\text{‰} \pm 1.9\text{‰}$
390 (mean \pm SD), and the $\delta^{15}\text{N}$ of TN was $3.2\text{‰} \pm 0.8\text{‰}$ (see Table S2 in the supplementary material
391 for details of elemental and stable isotopic signatures of mangrove leaves as end members for the
392 mixing model). The $\delta^{13}\text{C}$ values of POC from the FWEM and MEM were $-23.9\text{‰} \pm 0.1\text{‰}$ ($n =$
393 3) and $-21.8\text{‰} \pm 0.2\text{‰}$ ($n = 3$), respectively, whereas the $\delta^{15}\text{N}$ of PN were $6.0\text{‰} \pm 0.6\text{‰}$ ($n = 3$)
394 and $4.1\text{‰} \pm 0.2\text{‰}$ ($n = 3$), respectively. The isotopic and elemental signatures of organic matter



395 sources and bulk POM are presented in Fig. S2 (supplementary material). The results of the OM
396 mixing model using three parameters (including the N:C ratio) and using two parameters
397 (excluding the N:C ratio) are presented in Tables S3 and S4 (supplementary material).

398 The optical signatures $a_{CDOM(254)}$, $a_{CDOM(375)}$, and $SUVA_{254}$ showed a gradual decreasing trend
399 along with increasing salinity. However, no such trend was found for $S_{275-295}$. Most values for
400 $a_{CDOM(254)}$, $a_{CDOM(375)}$, and $SUVA_{254}$ plotted below the conservative mixing line, indicating that
401 their values were lower than the predicted conservative mixing values with a few exceptions,
402 mainly from the creeks (Fig. S3a–3c; supplementary material). In contrast, almost all of the S_{275-}
403 $_{295}$ values were higher than the predicted conservative mixing values with a sole exception from
404 MR (Fig. S3d, supplementary material).

405

406 **4. Discussion**

407 **4.1 Sinks and low effluxes of CO₂**

408 Although the narrow (and shallow) mangrove creeks acted as a weak source of CO₂, the
409 island boundary and middle of the river (which are within few metres of the creeks) clearly acted
410 as a net CO₂ sink. We compared the pCO₂(water) and air–water CO₂ flux with values of other
411 studies conducted around the world (Table 1). We considered only recent studies that used high-
412 resolution direct measurement of pCO₂(water) or direct measurement of air–water CO₂ flux for
413 this comparison. From the data in Table 1 it is evident that, except for our study, none of the
414 studies carried out in the waters around mangroves reported a negative flux; i.e. the waters in the
415 respective study areas did not act as a CO₂ sink. Moreover, in terms of the magnitude of the CO₂



416 source, our value for the creeks was much less than the CO₂ emission rates reported by other
417 studies.

418 If we consider only the mean CO₂ emission rate from the creeks (i.e. $1.6 \pm 4.3 \text{ mmol m}^{-2}$
419 d^{-1}), it is still lower by a factor of about 33 than the latest estimate of world average CO₂
420 emissions from the waters around mangroves ($56.8 \pm 8.9 \text{ mmol m}^{-2} \text{ d}^{-1}$; Rosentreter et al., 2018).
421 This low CO₂ flux value and the sink characteristics that we observed cannot be explained only
422 by proximity to a marine environment, because in similarly marine locations the waters
423 surrounding mangroves are a substantial source of CO₂.

424 **4.2 Effect of tidal pumping and pore water on pCO₂**

425 The waters around mangroves usually exhibit significant diel variability in terms of both
426 pCO₂(water) and air–water CO₂ flux, with higher pCO₂(water) values during low tide and vice-
427 versa (Zablocki et al., 2011). However, our continuous high-temporal-resolution measurements
428 showed that these changes in pCO₂(water) with respect to tides occurred only at the creek
429 stations (Fig. 2). Except for station IB1, none of the island boundary or mid-river stations
430 showed such distinct diel variability. The high pCO₂(water) during low tide is generally
431 attributed to pCO₂-rich pore water as well as groundwater, and the lower pCO₂(water) during
432 flood tide results from the dilution of mangrove-derived water with pCO₂-lean seawater (Maher
433 et al., 2013; Call et al., 2015; Akhand et al., 2016). The absence of pCO₂(water) maxima during
434 low tide at IB and MR stations indicates that the effect of pore water, which is prominent at the
435 creek stations, did not play a significant role in regulating the diel variation of pCO₂(water) at
436 these stations. This result might be due to the rapid transport of DIC-rich pore water by the



437 pCO₂-lean seawater leading to rapid dilution of DIC at IB and MR stations compared to stations
438 C1 and C2.

439 pCO₂(water) and DO usually show a negative correlation, as the consumption of
440 bicarbonate by phytoplankton during photosynthetic activity tends to convert pCO₂(water) to
441 bicarbonate ions [i.e. a decrease in pCO₂(water)] and produces oxygen. Because the temporal
442 resolution of DO measurements was much coarser than that of our pCO₂(water) data, we chose
443 not to perform a correlation analysis. However, it was clear that in the creeks where pCO₂(water)
444 was highest, the DO values were lowest, whereas the reverse was found at the MR stations. The
445 photosynthetic potential and composition of phytoplankton would not vary widely between these
446 stations because they are so close to each other. The atmospheric forcing that also plays a key role
447 in regulating DO in these waters also should not differ. Yet, even though the stations were close
448 to each other, the DO maxima during the midday hours (i.e. at the time of highest photosynthetic
449 photon flux) increased steadily from C to IB to MR stations. Hence, the difference in DO could be
450 attributed solely to the net heterotrophy exhibited by the water around the mangroves in the creeks
451 and the net autotrophic conditions at IB and MR. Furthermore, the pore water, which has a
452 prominent effect in the creeks, cannot promote the same level of heterotrophy when the water mass
453 is diluted by pCO₂-lean seawater.

454 **4.3 Mechanisms for influx or reduced efflux of CO₂**

455 The Revelle factor is the ratio of the relative change of pCO₂(water) to the corresponding
456 relative change of DIC in marine water (Egleston et al., 2010) and thus reflects the carbonate
457 buffering capacity of the water mass. Globally, the Revelle factor is found to vary between 8 (in
458 warm waters) and 15 (in cold waters) (Broecker et al., 1979). The lower the Revelle factor the



459 greater the capacity of the water to take up CO₂. In the present study the Revelle factor was
460 higher in the creeks than at mid-river and island-boundary stations, signifying a lower potential
461 for CO₂ uptake in the creeks than in the IB and MR waters. In other words, the unit increase in
462 pCO₂(water) with respect to the unit input of DIC was much higher at the creek stations than at
463 the IB and MR stations.

464 Taillardat et al. (2018) reported that in pore water, the longer residence time of water
465 coupled with greater water turnover enhances the solute fraction, which in turn increases the
466 pCO₂(water). This phenomenon was found to take place in the creeks, where in the absence of
467 rapid mixing, the mangrove water mass had a higher residence time compared to the island
468 boundary and mid-river, where the pore water underwent rapid dilution with pCO₂-lean seawater
469 leading to a reduced Revelle factor. The Revelle factor of the FWEM (26.7) was very high
470 compared to its values at the C, IB, or MR stations. Although the riverine freshwater supply is
471 limited in our study area, some ends up in the river mouth. Moreover, the estimated Revelle
472 factor of the pore water of Sundarban mangroves (computed from pore-water pH data of Mandal
473 et al. [2009] and pore-water DIC data of Dutta et al. [2019]) was also much higher (17.6) than
474 the Revelle factor in the creeks. Pore water is generated exclusively within the mangrove
475 environment.

476 In addition to pore water and freshwater, estuaries also often experience groundwater
477 seepage. The Revelle factor of groundwater in and around Sundarban mangroves was 14.9 ± 1.0
478 (unpublished data, Akhand et al.). However, the Revelle factors of riverine freshwater, pore
479 water and ground water were substantially higher than the Revelle factors at C, IB, and MR.
480 However, despite the higher Revelle factors for pore water, groundwater, and freshwater, the
481 waters around mangroves had lower values. The most likely explanation for such lower values is



482 the influence of marine water. The Revelle factor of the MEM (10.7) was substantially lower
483 than the factors in creek, island-boundary and mid-river waters. The Revelle factors farther
484 offshore in the BoB (almost to 10° N latitude) estimated from the TALK and DIC data of Goyet et
485 al. (1999) were only 8.9. When waters with such a low Revelle factor are mixed with the
486 groundwater, pore water, and freshwater at the C, IB, and MR stations, the resultant water
487 masses have an intermediate buffering capacity, between those of the FWEM and MEM. In other
488 words, the buffering capacity of the waters adjacent to mangroves is enhanced by mixing with
489 MEM waters.

490 Measured DIC in the present study ($2127 \pm 149 \mu\text{mol kg}^{-1}$ [mean \pm SD]; range, 2045–
491 2732 $\mu\text{mol kg}^{-1}$; $n = 31$) was in agreement with the reported DIC ranges from other mangrove-
492 associated waters that acted as net sources of CO₂ (Zablocki et al., 2011; Linto et al., 2014;
493 David et al., 2018; Ray et al., 2018b). DIC data from this study are comparable to DIC data
494 reported from other stations in the Indian Sundarbans (Ray et al., 2018a), where pCO₂(water)
495 data indicated that those sites might be sources of CO₂. In contrast, Dutta et al. (2019) observed
496 lower DIC values (1680–1920 $\mu\text{mol kg}^{-1}$) at various sites in the Indian Sundarbans during the
497 same post-monsoon season. Our plot of $\Delta\text{TALK}:\Delta\text{DIC}$ vs. ΔpCO_2 provides additional useful
498 insights into regulation of the pCO₂(water) concentration and subsequently the air–water CO₂
499 flux (Fig. 5a). This plot shows that, except for a few creek data, the buffering capacity was
500 mostly higher in the IB and MR waters. Hence, we conclude that the buffering capacity in the
501 study area is mainly governed by intruding pCO₂-lean water from the coastal ocean. The waters
502 around mangroves are known to have a buffering capacity against coastal acidification (Sippo et
503 al., 2016; Maher et al., 2018). In the present study, the data for the water around mangroves (and
504 the pore water or groundwater data from other studies) consistently show a TALK:DIC ratio >1,



505 which also supports this hypothesis. Moreover, as expected for BoB water, the buffering capacity
506 of the MEM predominates over the mangrove waters, further enhancing the CO₂ sink
507 characteristics of the waters adjacent to mangroves.

508 The $\delta^{13}\text{C}_{\text{DIC}}$ values (Fig. 3i) in the creeks were mostly lighter than the conservative
509 mixing estimates, a clear indication that the mangrove environment is the source of additional
510 DIC. The deviation plot (ΔDIC vs. $\Delta\delta^{13}\text{C}_{\text{DIC}}$; Fig. 5b) shows a positive ΔDIC with negative
511 $\Delta\delta^{13}\text{C}_{\text{DIC}}$, suggesting OM degradation and ground- and pore-water intrusion as the main sources
512 of DIC. A few data showed a slightly positive ΔDIC with positive $\Delta\delta^{13}\text{C}_{\text{DIC}}$ values, which
513 indicates carbonate dissolution. The most plausible explanation for the sources of the DIC is a
514 combination of mineralization of mangrove tissue ($-29.0\text{‰} \pm 1.9\text{‰}$, present study), degradation
515 and/or decomposition of POM in the water around mangroves ($\delta^{13}\text{C}_{\text{POC}} = -22.8\text{‰}$, [present
516 study]; -23.3‰ [Dutta et al., 2019]), groundwater- and pore water-derived DIC ($\delta^{13}\text{C}_{\text{DIC}} = -$
517 18.0‰ in Sundarban [Dutta et al., 2019]; -14.5‰ to -10.0‰ [Maher et al., 2013]), and
518 degradation and/or decomposition of marine phytoplankton ($\delta^{13}\text{C}_{\text{POC}} = -21.8\text{‰}$ [MEM, present
519 study]; -22.0‰ to -20.0‰ [Rosentreter et al., 2018]). However, we found no significant
520 correlation between $\delta^{13}\text{C}_{\text{DIC}}$ and $\delta^{13}\text{C}_{\text{POC}}$, which might be because the sources were well-mixed.

521 This type of mixed source has been found in other mangrove environments such as in
522 arid Red Sea mangroves (-11.2‰ to -15.9‰ ; $\delta^{13}\text{C}_{\text{DIC}}$; Sea et al., 2018) and on the north-eastern
523 coast of Queensland, Australia (-21.7‰ to -8.9‰ ; Rosentreter et al., 2018). In contrast to mixed
524 sources, the DIC of mangrove creek was found typically from the mangrove origin near North
525 Stradbroke Island, Australia (-29.4‰ ; Maher et al., 2017). However, Rosentreter et al. (2018)
526 stated that if, in fact, the emitted CO₂ was from an allochthonous carbon source, this would have
527 major implications for mangrove carbon budgets. In other words, under such a scenario the



528 carbon dynamics in the mangrove-associated waters cannot be completely explained solely by
529 mangrove-derived DIC loading, but is also regulated by other allochthonous sources.

530 Ray et al. (2018a) emphasized the rapid transport of material from Sundarban mangroves
531 to the BoB compared to other mangroves of the world. They assumed that the reason for this
532 rapid transport is the shorter residence time due to large tidal amplitudes. Because of the
533 estuarine geometry common in the Sundarbans, a “funnelling effect” tends to amplify the tide,
534 resulting in a further amplification of the tidal range and faster material transport (Ray et al.,
535 2018a). Recently Maher et al. (2018) revealed that the export of DIC and TAlk in a subtropical
536 mangrove system results in a long-term atmospheric carbon sink that is approximately 1.7 times
537 higher than burial and should be incorporated into the blue-carbon budget. Our observations
538 from the present study similarly indicates that the BoB could be a potential sink of the
539 mangrove-derived DIC and TAlk transported laterally from the Sundarbans.

540 The diagenesis of organic carbon in mangroves takes place through several anaerobic
541 pathways that increase pore-water TAlk (Koné and Borges, 2008). The relationship between
542 salinity-normalized DIC and salinity-normalized alkalinity (slope) can indicate the primary
543 biogeochemical processes that regulate the DIC and alkalinity dynamics (Borges et al., 2003;
544 Bouillon et al., 2007b). The salinity-normalized DIC and TAlk at our study site correlated well
545 ($r^2 = 0.98$; $n = 31$), having a slope of 0.84 (Fig. 6). The magnitude of the slope is apparently
546 close to that suggesting denitrification as observed in the waters around mangroves in the
547 Mekong Delta, Vietnam (Alongi et al., 2000) and Gaji Bay, Kenya (Bouillon et al., 2007a).
548 Denitrification has also been reported in the mangrove sediment of the Indian (Das et al., 2013;
549 Ray et al., 2014) and Bangladesh (Neogi et al., 2016) parts of the Sundarbans, and from the
550 mangrove environment of Goa (India), where it accounts for <0% to 72% of the pore-water



551 nitrate reduction (Fernandes et al., 2010, 2012). As the present study is the first of its kind in
552 Sundarbans, our results can be considered baseline data; no comparison with other parts of the
553 Sundarbans is possible, but this might be an avenue of future research. Although carbonate
554 dissolution is also evident from our NEC data, this was not a major pathway as is evident from
555 the deviation plot (ΔDIC vs. $\Delta\delta^{13}\text{C}_{\text{DIC}}$) (Fig. 4b) and the plot of salinity-normalized DIC vs.
556 TAlk (Fig. 6). Globally, denitrification is typically considered a minor diagenetic carbon
557 degradation pathway, with sulfate reduction and aerobic respiration often being the major
558 pathways in mangrove sediments (Alongi, 2005; Bouillon et al., 2007b).

559 The significantly negative NEP values indicate net heterotrophy at C2, which is also in
560 agreement with the mean CO_2 flux data, as this station acted as a net source of CO_2 . Also, a
561 significant negative NEC value indicates dissolution of calcium carbonate, as reported previously
562 in Sundarban (Ghosh et al., 1987) and the Hooghly estuaries (Samanta et al., 2015). Mangrove,
563 seagrass, and saltmarsh ecosystems are likely sites of net carbonate dissolution (Saderne et al.,
564 2019). Because the changes in DIC and TAlk at C2 could be explained by the photosynthesis–
565 irradiance curve, it is likely that biological metabolic activities, such as those NEP and NEC,
566 play a significant role in regulating the autochthonous DIC and TAlk. However, at the other
567 stations, the mixing of other water masses (leading to allochthonous input of DIC and TAlk) or
568 other unknown factors (see Tokoro et al., 2014) might be why the changes in DIC and TAlk
569 could not be explained by the photosynthesis–irradiance curve. To the best of our knowledge, the
570 present study is the first to estimate NEP and NEC in the waters around mangroves. Hence, these
571 are also baseline data and cannot yet be compared with other NEP and NEC data from water
572 around mangroves. However, Saderne et al. (2019) reported a burial rate for inorganic carbon of
573 0.8 in a mangrove ecosystem.



574 **4.4 Role of OM loading**

575 Although the organic carbon pool is not directly related to the air–water CO₂ flux, the
576 DOC and POC pools are important in discussions regarding the air–water CO₂ flux in mangrove
577 environments. One possible reason that mangrove waters function as a net CO₂ source is that the
578 water column and sediments receive substantial quantities of leaf and wood litter from the
579 overlying canopy and labile organic carbon is exported from mangroves to adjacent aquatic
580 systems (Borges et al., 2003). The loss of carbon (as DIC) mainly takes place through
581 mineralization of both DOC and POC, which are eventually exported into the estuaries and
582 oceans and finally to the atmosphere as CO₂ or CH₄ (Gattuso et al., 1998; Maher et al., 2013,
583 2015).

584 In the present study, DOC comprised the majority of the total organic carbon pool
585 (approx. 77%) and it was found to be added from within the mangrove surrounding water.
586 However, the concentrations of both DOC and POC in the present study are much lower ($104.5 \pm$
587 $18.7 \mu\text{M}$ and $30.7 \pm 11.6 \mu\text{M}$, respectively) than those observed at other mangrove sites around
588 the world. For example, DOC in mangroves along the Iranian coast of the Persian Gulf varies
589 between $296.2 \pm 22.7 \mu\text{M}$ and $332.1 \pm 45.6 \mu\text{M}$, whereas POC varies between $185.4 \pm 98.4 \mu\text{M}$
590 and $481.5 \pm 133 \mu\text{M}$ (Ray and Weigt, 2018). In the mangrove environment of French Guiana
591 (South America) the DOC and POC vary from 109 to 808 μM and 16.6 to 101 μM , respectively
592 (Ray et al., 2018b). In Moreton Bay, Australia, DOC is 80–200 μM and POC is 200–400 μM
593 (Maher et al., 2013). Although the POC concentrations in the present study are in agreement with
594 the reported ranges from other Sundarban sites ($32.0 \pm 8.5 \mu\text{M}$ [May] and $43.8 \pm 8.5 \mu\text{M}$
595 [December], Ray and Sahraki [2016]; 80–436 μM [post-monsoon season], Dutta et al. [2019]),
596 the DOC concentrations are substantially lower than not only other mangrove systems



597 worldwide, but also other study sites in the Sundarbans ($294.2 \pm 34.0 \mu\text{M}$ [May] and $262.0 \pm$
598 $43.7 \mu\text{M}$ [December], Ray and Sahraki [2016]; $154\text{--}315 \mu\text{M}$ [post-monsoon season], Dutta et al.
599 [2019]). POC and PN were well correlated, which suggests that they shared the same origin (Fig.
600 S4, supplementary material). Despite evidence of DOC addition in the system in our study, the
601 low concentrations might result from rapid transport towards the coastal sea, as previously
602 discussed in detail for DIC.

603 By comparing the results of two POM mixing models (with and without the N/C ratio)
604 obtained separately from C, IB, and MR data, it is clear that the contribution of POM from
605 mangroves gradually decreased from C to IB to MR, and at the same time there was an overall
606 lack of riverine freshwater contribution to the bulk POM. In contrast, the contribution of the
607 seawater end-member (marine phytoplankton) increased gradually in the same fashion. This
608 result indicates that mangroves in this region do contribute to the water-column POM; however,
609 it is quickly transported from the narrow mangrove creeks to the river and subsequently to the
610 coastal sea. The mixing model using $\delta^{13}\text{C}$, $\delta^{15}\text{N}$, and N/C revealed that the mangrove
611 contribution is low even in the creeks (median value, 17%; range, 2–44%). The mixing model
612 using only $\delta^{13}\text{C}$ and $\delta^{15}\text{N}$ (Table S4) revealed that in the creeks, the input of mangrove-derived
613 POM was 33% (6–69%), which is comparable to values from other studies in the Sundarbans (0–
614 65.3%; Ray et al., 2015). These results further indicate that if we only consider the model with
615 $\delta^{13}\text{C}$ and $\delta^{15}\text{N}$, then previous studies in the Sundarbans might have overestimated the mangrove
616 contribution to POM.

617 A unique feature of the DOM in the present study is that most of the DOC values plotted
618 above the conservative mixing line, indicating its addition within the system. In contrast, the
619 optical indicators $a_{\text{CDOM}(254)}$, $a_{\text{CDOM}(375)}$, and SUVA_{254} showed that almost all bulk CDOM plotted



620 below the conservative mixing line, indicating removal by the system. Both $a_{\text{CDOM}(254)}$ and
621 $a_{\text{CDOM}(375)}$ have been used in previous studies as metrics for the concentration of terrestrial
622 aromatic compounds (Weishaar et al., 2003; Zurbrugg et al., 2013) and as proxies for potential
623 refractory OM (Saadi et al., 2006; Hur et al., 2009). These optical signatures showed an overall
624 decrease with increases in salinity, i.e. from C towards MR. This result indicates an overall
625 decrease in the aromaticity of the DOM from the narrow creeks towards the coastal sea, whereas
626 Bergamaschi et al. (2012) reported that mangroves exude aromatic DOM. $S_{275-295}$ is used as an
627 optical indicator of potential terrestrial origin of CDOM (Fichot and Benner, 2012). Spencer et
628 al. (2012) suggested that increasing $S_{275-295}$ values are related to the decrease in molecular
629 weight and aromaticity of CDOM from fresh to marine waters. Almost all of the $S_{275-295}$ values
630 in the present study plotted above the conservative mixing line, indicating a lack of DOM of
631 freshwater origin. Moreover, the $S_{275-295}$ values in the present study were substantially higher
632 than the values reported by Ray et al. (2018b) for a mangrove environment in French Guiana
633 (South America), signifying less aromaticity of DOM than the typical mangrove-derived DOM.

634 **4.5 Seasonal and spatial up-scaling and comparison with global average CO₂ flux data**

635 We used the dataset of Akhand et al. (2016) for spatial and seasonal up-scaling and
636 updating of CO₂ flux data. They reported pCO₂(water) and CO₂ flux data for each month
637 annually and presented pre-monsoon (February–May), monsoon (June–September), and post-
638 monsoon (October–January) data from the upper, middle, and outer estuary of the Matla River.
639 Post-monsoon CO₂ flux was higher by a factor of about 9.6 and 13.3 in the middle and upper
640 estuary, respectively, than in the outer estuary. Similarly, the CO₂ flux was lower by a factor of
641 4.5 in the pre-monsoon season and 1.4 times higher in the monsoon season than in the post-
642 monsoon season. According to Akhand et al. (2016), the mean post-monsoon CO₂ flux in the



643 outer estuary was $-44 \mu\text{mol CO}_2 \text{ m}^{-2} \text{ h}^{-1}$, whereas in the present study (also post-monsoon and
644 outer estuary) the mean CO_2 flux over all eight stations was $-39.8 \mu\text{mol CO}_2 \text{ m}^{-2} \text{ h}^{-1}$. We used
645 the ratio of the flux value of Akhand et al. (2016) and the present study to up-scale and update
646 the CO_2 flux data for the whole estuary and for all seasons (throughout the year).

647 There are substantial differences between the methods used by Akhand et al. (2016) for
648 estimating and measuring $\text{pCO}_2(\text{water})$ and those in the present study, as well as between the
649 spatial and temporal resolution of the data. In addition, there might be differences between the
650 two studies due to interannual variation in the patterns of $\text{pCO}_2(\text{water})$ and other hydrological,
651 biogeochemical and meteorological conditions. Thus, the up-scaled CO_2 flux data should not be
652 used for their absolute values, which might have a higher uncertainty, but they can be useful for
653 comparison with globally averaged flux data.

654 On the basis of these criteria, we estimated the up-scaled CO_2 flux for the entire Matla
655 Estuary as $6.15 \text{ mmol m}^{-2} \text{ d}^{-1}$, which is much less than the world average for emissions from
656 mangrove-associated water ($56.8 \pm 8.9 \text{ mmol m}^{-2} \text{ d}^{-1}$; Rosentreter et al., 2018). We also
657 estimated the yearly CO_2 emission from the mangrove-associated waters of the Indian
658 Sundarbans using an area of 891 km^2 , encompassing freshwater domains closed to blind rivers
659 and creeks in the Sundarban biosphere of India (Dubey et al., 2015) as $88 \times 10^6 \text{ kg CO}_2 \text{ y}^{-1}$.

660 **5. Conclusions**

661 Our results suggest that the water around mangroves can sometimes act as a sink or a
662 weak source for CO_2 , contrary to most previous studies. Previous studies in the Sundarbans made
663 similar observations, but the precision and temporal resolution of the data were too coarse to
664 determine the source/sink characteristics. The present study successfully overcame the problems



665 and uncertainties with the earlier data by analysing the diel variability of pCO₂(water) at eight
666 sites covering the tidal maxima and minima and minimizing the possibility of over- or under-
667 estimation of CO₂ fluxes.

668 The elemental, stable isotopic, and optical signatures showed that the mangrove
669 ecosystem of the Sundarbans can contribute TAlk, DIC, DOC, and POC to the adjacent water (as
670 observed in other mangrove-associated waters around the globe); however, these carbon forms
671 are diluted by and transported to the pCO₂-lean coastal waters of the BoB. Moreover, stable
672 isotopic and optical signatures of this mangrove water showed negligible contributions from
673 riverine freshwater to the carbon input of this region. The minimal contribution of freshwater
674 input along with the predominance of pCO₂-lean northern BoB water increases the buffering
675 capacity, which, in turn, can explain the CO₂ sink properties of the waters surrounding the
676 Sundarban mangroves (or the reduced CO₂ efflux compared to global mangrove waters). Thus,
677 we argue that areas with such low emissions should be given due emphasis when up-scaling the
678 global mangrove carbon budget from regional observations.

679

680 **Data availability.** All data are available in this paper and supplementary material.

681

682 **Author contributions.** AA, AC, KW, SH, and TK designed the study. AA, AC, and SD did the
683 field work and sample collection. AA, AC, KW, SD, TT, and KC did the chemical and data
684 analysis. AA prepared the manuscript with input from AC and KW. SH and TK edited the
685 manuscript and provided all infrastructural facilities for this work. All authors read and approved
686 the manuscript.



687

688 **Competing interests.** The authors declare that they have no conflict of interest.

689

690 **Acknowledgements**

691 We are grateful for the funding of part of this work through the Environmental Research
692 and Technology Development Fund (S-14) and the Japan Society for the Promotion of Science
693 (KAKENHI 18H04156 and 19K20500). We also thank the National Remote Sensing Centre
694 (Department of Space, Government of India) for partial funding of this work. We also thank the
695 West Bengal Forest Department for granting us the necessary permissions. We are indebted to
696 Ms. N. Umegaki for help with the chemical analyses.

697

698 **References**

699

700 Adame, M.F., Lovelock, C.E.: Carbon and nutrient exchange of mangrove forests with the
701 coastal ocean, *Hydrobiologia*, 663(1), 23–50, <https://doi.org/10.1007/s10750-010-0554-7>,
702 2011.

703 Akhand, A., Chanda, A., Dutta, S., and Hazra, S.: Air–water carbon dioxide exchange dynamics
704 along the outer estuarine transition zone of Sundarban, northern Bay of Bengal, India, *Indian
705 J. Geomar. Sci.*, 41 (2), 111–116, 2012.

706 Akhand, A., Chanda, A., Dutta, S., Manna, S., Hazra, S., Mitra, D., Rao, K.H., and Dadhwal,
707 V.K.: Characterizing air–sea CO₂ exchange dynamics during winter in the coastal water off



- 708 the Hugli-Matla estuarine system in the northern Bay of Bengal, India, *J. Oceanogr.*, 69(6),
709 687–697, <https://doi.org/10.1007/s10872-013-0199-z>, 2013a.
- 710 Akhand, A., Chanda, A., Dutta, S., Manna, S., Sanyal, P., Hazra, S., Rao, K.H., and Dadhwal,
711 V.K.: Dual character of Sundarban estuary as a source and sink of CO₂ during summer: an
712 investigation of spatial dynamics, *Environ. Monit. Assess.*, 185(8), 6505–6515, DOI
713 10.1007/s10661-012-3042-x, 2013b.
- 714 Akhand, A., Chanda, A., Manna, S., Das, S., Hazra, S., Roy, R., Choudhury, S.B., Rao, K.H.,
715 Dadhwal, V.K., Chakraborty, K., and Mostofa, K.M.G., Tokoro, T., and Kuwae, T.: A
716 comparison of CO₂ dynamics and air–water fluxes in a river-dominated estuary and a
717 mangrove-dominated marine estuary, *Geophys. Res. Lett.*, 43(22), 11–726,
718 <https://doi.org/10.1002/2016GL070716>, 2016.
- 719 Alongi, D. M.: Mangrove-microbe-soil relations, in: *Interactions Between Macro- and*
720 *Microorganisms in Marine Sediments, Coastal Estuarine Stud.*, edited by: Kristensen, E.,
721 Kostka, J. E., and Haese, R. H., AGU, Washington, D. C., USA, 60, 85–103, 2005.
- 722 Alongi, D.M.: Carbon cycling and storage in mangrove forests, *Annu. Rev. Mar. Sci.*, 6, 195–
723 219, <https://doi.org/10.1146/annurev-marine-010213-135020>, 2014.
- 724 Alongi, D.M., Tirendi, F., Trott, L.A., and Xuan, T.T.: Benthic decomposition rates and
725 pathways in plantations of the mangrove *Rhizophora apiculata* in the Mekong delta,
726 Vietnam, *Mar. Ecol. Prog. Ser.*, 194, 87–101, doi:10.3354/meps194087, 2000.
- 727



- 728 Bergamaschi, B.A., Krabbenhoft, D.P., Aiken, G.R., Patino, E., Rumbold, D.G., and Orem,
729 W.H.: Tidally driven export of dissolved organic carbon, total mercury, and methylmercury
730 from a mangrove-dominated estuary, *Environ. Sci. Tech.*, 46(3), 1371–1378,
731 <https://doi.org/10.1021/es2029137>, 2012.
- 732 Biswas, H., Mukhopadhyay, S.K., De, T.K., Sen, S., and Jana, T.K.: Biogenic controls on the
733 air–water carbon dioxide exchange in the Sundarban mangrove environment, northeast coast
734 of Bay of Bengal, India, *Limnol. Oceanogr.*, 49(1), 95–101,
735 <https://doi.org/10.4319/lo.2004.49.1.0095>, 2004.
- 736 Borges, A.V., and Abril, G.: Carbon Dioxide and Methane Dynamics in Estuaries, in: *Treatise on*
737 *Estuarine and Coastal Science*, edited by: Wolanski, E., and McLusky, D.S., Waltham:
738 Academic Press, Elsevier Inc., 119–161, 5, DOI: 10.1016/B978-0-12-374711-2.00504-0,
739 2011.
- 740 Borges, A.V., Djenidi, S., Lacroix, G., Théate, J., Delille, B., and Frankignoulle, M.:
741 Atmospheric CO₂ flux from mangrove surrounding waters, *Geophys. Res. Lett.*, 30(11),
742 <https://doi.org/10.1029/2003GL017143>, 2003.
- 743 Borges, A.V., Delille, B., and Frankignoulle, M.: Budgeting sinks and sources of CO₂ in the
744 coastal ocean: Diversity of ecosystems counts, *Geophys. Res.*
745 *Lett.*, 32(14), <https://doi.org/10.1029/2005GL023053>, 2005.
- 746 Borges, A.V., Abril, G., and Bouillon, S.: Carbon dynamics and CO₂ and CH₄ outgassing in the
747 Mekong delta, *Biogeosci.*, 15(4), 1093–1114, <https://doi.org/10.5194/bg-15-1093-2018>, 2018.
- 748



- 749 Bouillon, S., and Boschker, H.T.S.: Bacterial carbon sources in coastal sediments: a cross-system
750 analysis based on stable isotope data of biomarkers, *Biogeosciences*, 3, 175–185,
751 <https://doi.org/10.5194/bg-3-175-2006>, 2006.
- 752 Bouillon, S., Dehairs, F., Velimirov, B., Abril, G., and Borges, A.V.: Dynamics of organic and
753 inorganic carbon across contiguous mangrove and seagrass systems (Gazi Bay, Kenya), *J.*
754 *Geophys. Res.: Biogeosci.*, 112(G02018), <https://doi.org/10.1029/2006JG000325>, 2007a.
- 755 Bouillon, S., Middelburg, J.J., Dehairs, F., Borges, A.V., Abril, G., Flindt, M.R., Ulomi, S., and
756 Kristensen, E.: Importance of intertidal sediment processes and porewater exchange on the
757 water column biogeochemistry in a pristine mangrove creek (Ras Dege,
758 Tanzania), *Biogeosciences*, 4, 311–322, <https://doi.org/10.5194/bg-4-311-2007>, 2007b.
- 759 Bouillon, S., Connolly, R.M., and Lee, S.Y.: Organic matter exchange and cycling in mangrove
760 ecosystems: recent insights from stable isotope studies, *J. Sea Res.*, 59(1–2), 44–58,
761 <https://doi.org/10.1016/j.seares.2007.05.001>, 2008.
- 762 Breithaupt, J.L., Smoak, J.M., Smith III, T.J., Sanders, C.J., and Hoare, A.: Organic carbon
763 burial rates in mangrove sediments: Strengthening the global budget, *Glob. Biogeochem.*
764 *Cycles*, 26(GB3011), <https://doi.org/10.1029/2012GB004375>, 2012.
- 765 Broecker, W.S., Takahashi, T., Simpson, H.J., and Peng, T.H.: Fate of fossil fuel carbon dioxide
766 and the global carbon budget, *Science*, 206(4417), 409–418, DOI:
767 10.1126/science.206.4417.409, 1979.
- 768 Call, M., Maher, D.T., Santos, I.R., Ruiz-Halpern, S., Mangion, P., Sanders, C.J., Erler, D.V.,
769 Oakes, J.M., Rosentreter, J., Murray, R., and Eyre, B.D.: Spatial and temporal variability of



- 770 carbon dioxide and methane fluxes over semi-diurnal and spring–neap–spring timescales in a
771 mangrove creek, *Geochim. Cosmochim. Acta*, 150, 211–225,
772 <https://doi.org/10.1016/j.gca.2014.11.023>, 2015.
- 773 Call, M., Santos, I.R., Dittmar, T., de Rezende, C.E., Asp, N.E., and Maher, D.T.: High pore-
774 water derived CO₂ and CH₄ emissions from a macro-tidal mangrove creek in the Amazon
775 region, *Geochim. Cosmochim. Acta*, 247, 106-120, <https://doi.org/10.1016/j.gca.2018.12.029>,
776 2019.
- 777 Chakrabarti, P.S.: Changing courses of Ganga, Ganga–Padma river system, West Bengal, India–
778 RS data usage in user orientation, river behavior and control, *J. River Res. Instit.*, 25, 19–40,
779 1998.
- 780 Cole, C.V., and Vaidyaraman, P.P.: Salinity distribution and effect of freshwater flows in the
781 Hooghly River, in: *Proceedings of the 10th Conference on Coastal Engineering*, Tokyo, Japan
782 (American Society of Civil Engineers, New York), September 1966, 1312–1434, 1966.
- 783 Das, S., Ganguly, D., Maiti, T.K., Mukherjee, A., Jana, T.K., and De, T.K.: A depth wise
784 diversity of free living N₂ fixing and nitrifying bacteria and its seasonal variation with nitrogen
785 containing nutrients in the mangrove sediments of Sundarban, WB, India, *Open J. Mar.*
786 *Sci.*, 3(02), 112–119, <http://dx.doi.org/10.4236/ojms.2013.32012>, 2013.
- 787 David, F., Meziane, T., Tran-Thi, N.T., Van, V.T., Thanh-Nho, N., Taillardat, P., and Marchand,
788 C.: Carbon biogeochemistry and CO₂ emissions in a human impacted and mangrove
789 dominated tropical estuary (Can Gio, Vietnam), *Biogeochemistry*, 138, 261–275,
790 <https://doi.org/10.1007/s10533-018-0444-z>, 2018.



- 791 Dickson, A.G., Sabine, C.L. and Christian, J.R. (Eds.): Guide to Best Practices for Ocean CO₂
792 Measurements, PICES Special Publication, North Pacific Marine Science Organization,
793 Canada, 2007.
- 794 Donato, D.C., Kauffman, J.B., Murdiyarso, D., Kurnianto, S., Stidham, M., and Kanninen, M.:
795 Mangroves among the most carbon-rich forests in the tropics, *Nat. Geosci.*, 4(5), 293, DOI:
796 10.1038/NGEO1123, 2011.
- 797 Dubey, S.K., Trivedi, R.K., and Chand, B.K.: Indigenous freshwater piscine resources of Indian
798 Sundarban biosphere reserve: status and prospects, *World J. Fish Mar. Sci.*, 7(1), 21–28, DOI:
799 10.5829/idosi.wjfm.2015.7.1.92103, 2015.
- 800 Dutta, M.K., Kumar, S., Mukherjee, R., Sanyal, P., and Mukhopadhyay, S.K.: The post-monsoon
801 carbon biogeochemistry of the Hooghly–Sundarbans estuarine system under different levels of
802 anthropogenic impacts, *Biogeosciences*, 16(2), 289–307, [https://doi.org/10.5194/bg-16-289-](https://doi.org/10.5194/bg-16-289-2019)
803 2019, 2019.
- 804 Egleston, E.S., Sabine, C.L., and Morel, F.M.: Revelle revisited: Buffer factors that quantify the
805 response of ocean chemistry to changes in DIC and alkalinity, *Glob. Biogeochem.*
806 *Cycles*, 24(1), <https://doi.org/10.1029/2008GB003407>, 2010.
- 807 Fernandes, S.O., Bharathi, P.A., Bonin, P.C., and Michotey, V.D.: Denitrification: an important
808 pathway for nitrous oxide production in tropical mangrove sediments (Goa, India). *J. Environ.*
809 *Qual.*, 39(4), 1507–1516, 2010.



- 810 Fernandes, S.O., Bonin, P.C., Michotey, V.D., Garcia, N., and LokaBharathi, P.A.: Nitrogen-
811 limited mangrove ecosystems conserve N through dissimilatory nitrate reduction to
812 ammonium, *Sci. Rep.*, 2, 419, <https://doi.org/10.1038/srep00419>, 2012.
- 813 Fichot, C.G., and Benner, R.: The spectral slope coefficient of chromophoric dissolved organic
814 matter ($S_{275-295}$) as a tracer of terrigenous dissolved organic carbon in river-influenced ocean
815 margins, *Limnol. Oceanogr.*, 57(5), 1453–1466, <https://doi.org/10.4319/lo.2012.57.5.1453>,
816 2012.
- 817 Friis, K., Körtzinger, A., and Wallace, D.W.: The salinity normalization of marine inorganic
818 carbon chemistry data, *Geophys. Res. Lett.*, 30(2), <https://doi.org/10.1029/2002GL015898>,
819 2003.
- 820 Fuentes, J.D., and Barr JG.: Mangrove forests and carbon and water cycling, *Agric. For.*
821 *Meteorol.*, 213, 263–265, DOI: 10.1016/j.agrformet.2015.08.243, 2015.
- 822 Gattuso, J.P., Frankignoulle, M., and Wollast, R.: Carbon and carbonate metabolism in coastal
823 aquatic ecosystems, *Annu. Rev. Ecol. Syst.*, 29(1), 405–434,
824 <https://doi.org/10.1146/annurev.ecolsys.29.1.405>, 1998.
- 825 Ghosh, S., Jana, T.K., Singh, B.N., and Choudhury, A.: Comparative study of carbon dioxide
826 system in virgin and reclaimed mangrove waters of Sundarban during freshet, *Bull. Nat. Instit.*
827 *Oceanogr.*, 20(3), 155–161, 1987.
- 828 Giri, C., Ochieng, E., Tieszen, L.L., Zhu, Z., Singh, A., Loveland, T., Masek, J., and Duke, N.:
829 Status and distribution of mangrove forests of the world using earth observation satellite



- 830 data, *Glob. Ecol. Biogeogr.*, 20(1), 154–159, <https://doi.org/10.1111/j.1466->
831 8238.2010.00584.x, 2011.
- 832 Gleeson, J., Santos, I.R., Maher, D.T., and Golsby-Smith, L.: Groundwater–surface water
833 exchange in a mangrove tidal creek: evidence from natural geochemical tracers and
834 implications for nutrient budgets, *Mar. Chem.*, 156, 27–37,
835 <https://doi.org/10.1016/j.marchem.2013.02.001>, 2013.
- 836 Gopal, B., and Chauhan, M.: Biodiversity and its conservation in the Sundarban mangrove
837 ecosystem. *Aquat. Sci.*, 68(3), 338–354, <https://doi.org/10.1007/s00027-006-0868-8>, 2006.
- 838 Goyet, C., Coatanoan, C., Eiseheid, G., Amaoka, T., Okuda, K., Healy, R., and Tsunogai, S.:
839 Spatial variation of total CO₂ and total alkalinity in the northern Indian Ocean: A novel
840 approach for the quantification of anthropogenic CO₂ in seawater, *J. Mar. Res.*, 57(1), 135–
841 163, <https://doi.org/10.1357/002224099765038599>, 1999.
- 842 Ho, D.T., Schlosser, P., and Orton, P.M.: On factors controlling air–water gas exchange in a
843 large tidal river, *Estuaries Coast.*, 34(6), 1103–1116, <https://doi.org/10.1007/s12237-011->
844 9396-4, 2011.
- 845 Ho, D.T., Ferrón, S., Engel, V.C., Larsen, L.G., and Barr, J.G.: Air–water gas exchange and CO₂
846 flux in a mangrove-dominated estuary, *Geophys. Res. Lett.*, 41(1), 108–113,
847 <https://doi.org/10.1002/2013GL058785>, 2014.
- 848 Hur J., Park, M.H., and Schlautman, M.A.: Microbial transformation of dissolved leaf litter
849 organic matter and its effects on selected organic matter operational descriptors, *Environ. Sci.*
850 *Tech.*, 43(7), 2315–2321, <https://doi.org/10.1021/es802773b>, 2009.



- 851 [IPCC] Intergovernmental Panel on Climate Change, Pachauri, R.K., and Meyer, L.A. (Eds.):
852 Climate Change 2014: Synthesis Report, Contribution of Working Groups I, II and III to the
853 Fifth Assessment Report of the Intergovernmental Panel on Climate Change, Core Writing
854 Team (IPCC), Geneva, Switzerland, 151 pp., 2014.
- 855 Jacotot, A., Marchand, C., and Allenbach, M.: Tidal variability of CO₂ and CH₄ emissions from
856 the water column within a Rhizophora mangrove forest (New Caledonia), *Sci. Tot.*
857 *Environ.*, 631, 334-340, <https://doi.org/10.1016/j.scitotenv.2018.03.006>, 2018.
- 858 Jennerjahn, T.C., and Ittekkot, V.: Relevance of mangroves for the production and deposition of
859 organic matter along tropical continental margins, *Naturwissenschaften*, 89(1), 23–30,
860 <https://doi.org/10.1007/s00114-001-0283-x>, 2002.
- 861 Kayanne, H., Suzuki, A., and Saito, H.: Diurnal changes in the partial pressure of carbon dioxide
862 in coral reef water, *Science*, 269(5221), 214–216, DOI: 10.1126/science.269.5221.214, 1995.
- 863 Kondo J.: *Atmosphere Science near the Ground Surface*, University of Tokyo Press, Tokyo,
864 Japan, 2000.
- 865 Koné, Y.M., and Borges, A.V.: Dissolved inorganic carbon dynamics in the waters surrounding
866 forested mangroves of the Ca Mau Province (Vietnam), *Estuar. Coast. Shelf Sci.*, 77(3), 409–
867 421, <https://doi.org/10.1016/j.ecss.2007.10.001>, 2008.
- 868 Kristensen, E., and Alongi, D.M.: Control by fiddler crabs (*Uca vocans*) and plant roots
869 (*Avicennia marina*) on carbon, iron, and sulfur biogeochemistry in mangrove
870 sediment, *Limnol. Oceanogr.*, 51(4), 1557–1571. 2006.



- 871 Kristensen, E., Flindt, M.R., Ulomi, S., Borges, A.V., Abril, G., and Bouillon, S.: Emission of
872 CO₂ and CH₄ to the atmosphere by sediments and open waters in two Tanzanian mangrove
873 forests, *Mar. Ecol. Prog. Ser.*, 370, 53–67, doi: 10.3354/meps07642, 2008.
- 874 Krumins, V., M. Gehlen, S. Arndt, P. Van Cappellen, and P. Regnier (2013), Dissolved
875 inorganic carbon and alkalinity fluxes from coastal marine sediments: Model estimates for
876 different shelf environments and sensitivity to global change, *Biogeosciences*, 10(1), 371–398,
877 doi:10.5194/bg-10-371-2013
- 878 Lekphet, S., Nitorisavut, S., and Adsavakulchai, S.: Estimating methane emissions from
879 mangrove area in Ranong Province, Thailand, *Songklanakarin J. Sci. Tech.*, 27(1), 153–163,
880 2005.
- 881 Li, X., Hu, B.X., Burnett, W.C., Santos, I.R., and Chanton, J.P.: Submarine groundwater
882 discharge driven by tidal pumping in a heterogeneous aquifer, *Groundwater*, 47(4), 558–
883 568, <https://doi.org/10.1111/j.1745-6584.2009.00563.x>, 2009.
- 884 Linto, N., Barnes, J., Ramachandran, R., Divia, J., Ramachandran, P., Upstill-Goddard, R.C.:
885 Carbon dioxide and methane emissions from mangrove-associated waters of the Andaman
886 Islands, Bay of Bengal, *Estuaries Coast.*, 37(2), 381–398, DOI 10.1007/s12237-013-9674-4,
887 2014.
- 888 Macklin, P.A., Suryaputra, I.G.N.A., Maher, D.T., Murdiyarso, D., and Santos, I.R.: Drivers of
889 CO₂ along a mangrove-seagrass transect in a tropical bay: Delayed groundwater seepage and
890 seagrass uptake, *Cont. Shelf Res.*, 172, 57-67, <https://doi.org/10.1016/j.csr.2018.10.008>, 2019.



- 891 Macreadie, P.I., Anton, A., Raven, J.A., Beaumont, N., Connolly, R.M., Friess, D.A., Kelleway,
892 J.J., Kennedy, H., Kuwae, T., Lavery, P.S., Lovelock, C.E., Smale, D.A., Apostolaki, E.T.,
893 Atwood, T.B., Baldock, J., Bianchi, T.S., Chmura, G.L., Eyre, B.D., Fourqurean, J.W., Hall-
894 Spencer, J.M., Huxham, M., Hendriks, I.E., Krause-Jensen, D., Laffoley, D., Luisetti, T.,
895 Marbà, N., Masque, P., McGlathery, K.J., Megonigal, J.P., Murdiyarso, Russell, B.D., Santos,
896 R., Serrano, O., Silliman, B.R., Watanabe, K., and Duarte, C.M.: The future of Blue Carbon
897 science, *Nat., Commun.*, 10(1), 1–13, <https://doi.org/10.1038/s41467-019-11693-w>, 2019.
- 898 Maher, D.T., Santos, I.R., Golsby-Smith, L., Gleeson, J., Eyre, B.D.: Groundwater-derived
899 dissolved inorganic and organic carbon exports from a mangrove tidal creek: The missing
900 mangrove carbon sink?, *Limnol. Oceanogr.*, 58(2), 475–
901 488, <https://doi.org/10.4319/lo.2013.58.2.0475>, 2013.
- 902 Maher, D.T., Cowley, K., Santos, I.R., Macklin, P., Eyre, B.D.: Methane and carbon dioxide
903 dynamics in a subtropical estuary over a diel cycle: Insights from automated in situ radioactive
904 and stable isotope measurements, *Mar. Chem.*, 168, 69–79,
905 <https://doi.org/10.1016/j.marchem.2014.10.017>, 2015.
- 906 Maher, D.T., Santos, I.R., Schulz, K.G., Call, M., Jacobsen, G.E., and Sanders, C.J.: Blue carbon
907 oxidation revealed by radiogenic and stable isotopes in a mangrove system, *Geophys. Res.*
908 *Lett.*, 44(10), 4889–4896, <https://doi.org/10.1002/2017GL073753>, 2017.
- 909 Maher, D.T., Call, M., Santos, I.R., and Sanders, C.J.: Beyond burial: lateral exchange is a
910 significant atmospheric carbon sink in mangrove forests, *Biol. Lett.*, 14(7), 20180200,
911 <https://doi.org/10.1098/rsbl.2018.0200>, 2018.



- 912 Mandal, S.K., Dey, M., Ganguly, D., Sen, S., and Jana, T.K.: Biogeochemical controls of arsenic
913 occurrence and mobility in the Indian Sundarban mangrove ecosystem, *Mar. Pollut.*
914 *Bull.*, 58(5), 652–657, <https://doi.org/10.1016/j.marpolbul.2009.01.010>, 2009.
- 915 Mcleod, E., Chmura, G.L., Bouillon, S., Salm, R., Björk, M., Duarte, C.M., Lovelock, C.E.,
916 Schlesinger, W.H., and Silliman, B.R., A blueprint for blue carbon: toward an improved
917 understanding of the role of vegetated coastal habitats in sequestering CO₂, *Front. Ecol.*
918 *Environ.*, 9(10), 552–560, <https://doi.org/10.1890/110004>, 2011.
- 919 Mitra, A., Banerjee, K., Sengupta, K., and Gangopadhyay, A.: Pulse of Climate Change in Indian
920 Sundarbans: A Myth or Reality?, *Natl. Acad. Sci. Lett. (India)*, 32(1),19, 2009.
- 921 Miyajima, T., Miyajima, Y., Hanba, Y.T., Yoshii, K., Koitabashi, T., and Wada, E.: Determining
922 the stable isotope ratio of total dissolved inorganic carbon in lake water by
923 GC/C/IRMS, *Limnol. Oceanogr.*, 40(5), 994–1000,
924 <https://doi.org/10.4319/lo.1995.40.5.0994>, 1995.
- 925 Mook, W.G., Tan, T.C.: Stable carbon isotopes in rivers and estuaries, in: *Biogeochemistry of*
926 *Major World Rivers*, edited by: Degens, E.T., Kempe, S., and Richey, J.E., SCOPE, John
927 Wiley and Sons Ltd., 245–264. 1991.
- 928 Neogi, S.B., Dey, M., Lutful Kabir, S.M., Masum, S.J.H., Kopprio, G.A., Yamasaki, S., and
929 Lara, R.J.: Sundarban mangroves: diversity, ecosystem services and climate change impacts,
930 *Asian J. Med. Biol. Res.*, 2 (4), 488–507, 2016.



- 931 Parnell, A.C., Inger, R., Bearhop, S., and Jackson, A.L.: Source partitioning using stable
932 isotopes: coping with too much variation, *PloS One*, 5(3), e9672,
933 <https://doi.org/10.1371/journal.pone.0009672>, 2010.
- 934 Pendleton, L., Donato, D.C., Murray, B.C., Crooks, S., Jenkins, W.A., Sifleet, S., Craft, C.,
935 Fourqurean, J.W., Kauffman, J.B., Marbà, N., and Megonigal, P.: Estimating global “blue
936 carbon” emissions from conversion and degradation of vegetated coastal ecosystems, *PloS*
937 *one*, 7(9), e43542, <https://doi.org/10.1371/journal.pone.0043542>, 2012.
- 938 Ray, R., and Shahraki, M.: Multiple sources driving the organic matter dynamics in two
939 contrasting tropical mangroves, *Sci. Total Environ.*, 571, 218–227,
940 <https://doi.org/10.1016/j.scitotenv.2016.07.157>, 2016.
- 941 Ray, R., Weigt, M.: Seasonal and habitat-wise variations of creek water particulate and dissolved
942 organic carbon in arid mangrove (the Persian Gulf), *Cont. Shelf Res.*, 165, 60–70,
943 <https://doi.org/10.1016/j.csr.2018.06.009>, 2018.
- 944 Ray, R., Majumder, N., Das, S., Chowdhury, C., and Jana, T.K.: Biogeochemical cycle of
945 nitrogen in a tropical mangrove ecosystem, east coast of India. *Marine Chemistry*, 167, 33–43,
946 <https://doi.org/10.1016/j.marchem.2014.04.007>, 2014.
- 947 Ray, R., Rixen, T., Baum, A., Malik, A., Gleixner, G., and Jana, T.K.: Distribution, sources and
948 biogeochemistry of organic matter in a mangrove dominated estuarine system (Indian
949 Sundarbans) during the pre-monsoon, *Estuar. Coast. Shelf Sci.*, 167, 404–413,
950 <https://doi.org/10.1016/j.ecss.2015.10.017>, 2015.



- 951 Ray, R., Baum, A., Rixen, T., Gleixner, G., and Jana, T.K.: Exportation of dissolved (inorganic
952 and organic) and particulate carbon from mangroves and its implication to the carbon budget
953 in the Indian Sundarbans, *Sci. Total. Environ.*, 621, 535–547,
954 <https://doi.org/10.1016/j.scitotenv.2017.11.225>, 2018a.
- 955 Ray, R., Michaud, E., Aller, R.C., Vantrepotte, V., Gleixner, G., Walcker, R., Devesa, J., Le
956 Goff, M., Morvan, S., and Thouzeau, G.: The sources and distribution of carbon (DOC, POC,
957 DIC) in a mangrove dominated estuary (French Guiana, South
958 America), *Biogeochemistry*, 138(3), 297–321, <https://doi.org/10.1007/s10533-018-0447-9>,
959 2018b.
- 960 Robinson, C., Li, L., and Prommer, H.: Tide-induced recirculation across the aquifer-ocean
961 interface, *Water Resour. Res.*, 43(7), <https://doi.org/10.1029/2006WR005679>, 2007.
- 962 Rosentreter, J.A., Maher, D.T., Erler, D.V., Murray, R., and Eyre, B.D.: Seasonal and temporal
963 CO₂ dynamics in three tropical mangrove creeks – A revision of global mangrove CO₂
964 emissions, *Geochim. Cosmochim. Acta*, 222, 729–745,
965 <https://doi.org/10.1016/j.gca.2017.11.026>, 2018.
- 966 Saadi, I., Borisover, M., Armon, R., and Laor, Y.: Monitoring of effluent DOM biodegradation
967 using fluorescence, UV and DOC measurements, *Chemosphere*, 63(3), 530–539,
968 <https://doi.org/10.1016/j.chemosphere.2005.07.075>, 2006.
- 969 Saderne, V., Geraldi, N.R., Macreadie, P.I., Maher, D.T., Middelburg, J.J., Serrano, O.,
970 Almahasheer, H., Arias-Ortiz, A., Cusack, M., Eyre, B.D., Fourqurean, J.W., Kennedy, H.,
971 Krause-Jensen, D., Kuwae, T., Lavery, P.S., Lovelock, C.E., Marba, N., Masqué, P., Mateo,
972 M.A., Mazarrasa, I., McGlathery, K.J., Oreska, M.P.J., Sanders, C.J., Santos, I.R., Smoak,



- 973 J.M., Tanaya, T., Watanabe, K., and Duarte, C.M.: Role of carbonate burial in Blue Carbon
974 budgets, *Nat. Commun.*, 10(1), 1106, <https://doi.org/10.1038/s41467-019-08842-6>, 2019.
- 975 Saito, H., Tamura, N., Kitano, H., Mito, A., Takahashi, C., Suzuki, A., and Kayanne, H.: A
976 compact seawater pCO₂ measurement system with membrane equilibrator and nondispersive
977 infrared gas analyzer, *Deep Sea Res. Part I: Oceanogr. Res. Pap.*, 42(11–12), 2025–2033,
978 [https://doi.org/10.1016/0967-0637\(95\)00090-9](https://doi.org/10.1016/0967-0637(95)00090-9), 1995.
- 979 Samanta, S., Dalai, T.K., Pattanaik, J.K., Rai, S.K., and Mazumdar, A.: Dissolved inorganic
980 carbon (DIC) and its δ₁₃C in the Ganga (Hooghly) River estuary, India: Evidence of DIC
981 generation via organic carbon degradation and carbonate dissolution, *Geochim. Cosmochim.*
982 *Acta*, 165, 226–248, <https://doi.org/10.1016/j.gca.2015.05.040>, 2015.
- 983 Sanders, C.J., Maher, D.T., Tait, D.R., Williams, D., Holloway, C., Sippo, J.Z., and Santos, I.R.:
984 Are global mangrove carbon stocks driven by rainfall?, *J. Geophys. Res.: Biogeosci.*, 121(10),
985 2600–2609, <https://doi.org/10.1002/2016JG003510>, 2016a.
- 986 Sanders, C.J., Santos, I.R., Maher, D.T., Breithaupt, J.L., Smoak, J.M., Ketterer, M., Call, M.,
987 Sanders, L., and Eyre, B.D.: Examining ²³⁹⁺²⁴⁰Pu, ²¹⁰Pb and historical events to determine
988 carbon, nitrogen and phosphorus burial in mangrove sediments of Moreton Bay, Australia, *J.*
989 *Environ. Radioact.*, 151, 623–629, <https://doi.org/10.1016/j.jenvrad.2015.04.018>, 2016b.
- 990 Santos, I.R., Eyre, B.D., and Huettel, M.: The driving forces of porewater and groundwater flow
991 in permeable coastal sediments: A review, *Estuarine, Coast. Shelf Sci.*, 98, 1–15,
992 <https://doi.org/10.1016/j.ecss.2011.10.024>, 2012.



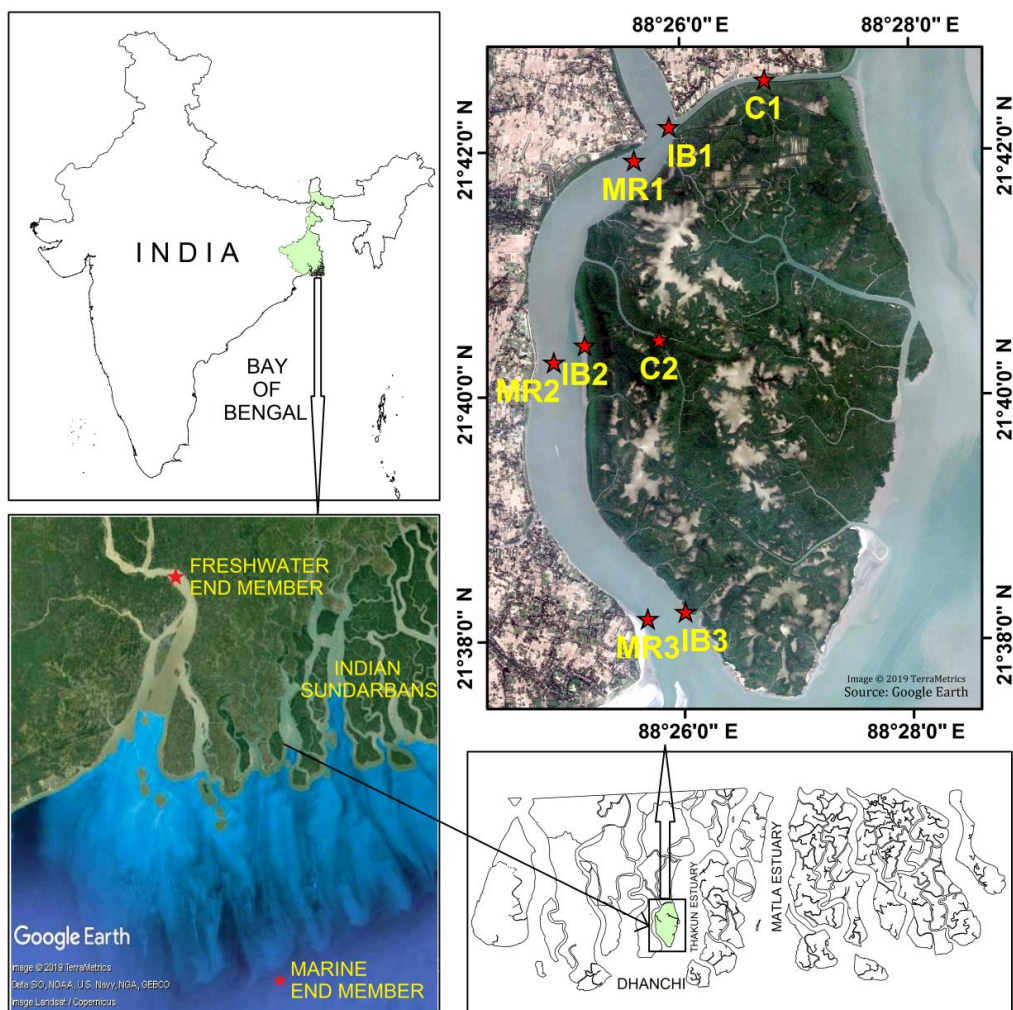
- 993 Sarkar, S.K., Frančišković-Bilinski, S., Bhattacharya, A., Saha, M., and Bilinski, H.: Levels of
994 elements in the surficial estuarine sediments of the Hugli River, northeast India and their
995 environmental implications, *Environ. Int.*, 30(8), 1089–1098,
996 <https://doi.org/10.1016/j.envint.2004.06.005>, 2004.
- 997 Sea, M.A., Garcias-Bonet, N., Saderne, V., and Duarte, C.M.: Carbon dioxide and methane
998 fluxes at the air–sea interface of Red Sea mangroves, *Biogeosciences*, 15, 5365–5375,
999 <https://doi.org/10.5194/bg-15-5365-2018>, 2018.
- 1000 Sippo, J.Z., Maher, D.T., Tait, D.R., Holloway, C., and Santos, I.R.: Are mangroves drivers or
1001 buffers of coastal acidification? Insights from alkalinity and dissolved inorganic carbon export
1002 estimates across a latitudinal transect, *Glob. Biogeochem. Cycles*, 30(5), 753–766,
1003 <https://doi.org/10.1002/2015GB005324>, 2016.
- 1004 Spencer, R.G., Butler, K.D., Aiken, G.R.: Dissolved organic carbon and chromophoric dissolved
1005 organic matter properties of rivers in the USA, *J. Geophys. Res.: Biogeosci.*, 117(G3),
1006 <https://doi.org/10.1029/2011JG001928>, 2012.
- 1007 Taillardat, P., Ziegler, A.D., Friess, D.A., Widory, D., Van, V.T., David, F., Thành-Nho, N., and
1008 Marchand, C.: Carbon dynamics and inconstant porewater input in a mangrove tidal creek
1009 over contrasting seasons and tidal amplitudes, *Geochim. Cosmochim. Acta*, 237, 32–48,
1010 <https://doi.org/10.1016/j.gca.2018.06.012>, 2018.
- 1011 Tokoro, T., Hosokawa, S., Miyoshi, E., Tada, K., Watanabe, K., Montani, S., Kayanne, H., and
1012 Kuwae, T.: Net uptake of atmospheric CO₂ by coastal submerged aquatic vegetation, *Glob.*
1013 *Change Biol.*, 20(6), 1873–1884, <https://doi.org/10.1111/gcb.12543>, 2014.



- 1014 Twilley, R.R., Chen, R.H., Hargis, T.: Carbon sinks in mangroves and their implications to
1015 carbon budget of tropical coastal ecosystems, *Water, Air, Soil Pollut.*, 64(1–2), 265–288,
1016 <https://doi.org/10.1007/BF00477106>, 1992.
- 1017 Wanninkhof, R.: Relationship between wind speed and gas exchange over the ocean
1018 revisited, *Limnol. Oceanogr.: Method.*, 12(6), 351–
1019 362, <https://doi.org/10.4319/lom.2014.12.351>, 2014.
- 1020 Weishaar, J.L., Aiken, G.R., Bergamaschi, B.A., Fram, M.S., Fujii, R., and Mopper, K.:
1021 Evaluation of specific ultraviolet absorbance as an indicator of the chemical composition and
1022 reactivity of dissolved organic carbon, *Environ. Sci. Tech.*, 37(20), 4702–4708,
1023 <https://doi.org/10.1021/es030360x>, 2003.
- 1024 Weiss, R.: Carbon dioxide in water and seawater: the solubility of a non-ideal gas, *Mar.*
1025 *Chem.*, 2(3), 203–215, [https://doi.org/10.1016/0304-4203\(74\)90015-2](https://doi.org/10.1016/0304-4203(74)90015-2), 1974.
- 1026 Zablocki, J.A., Andersson, A.J., and Bates, N.R.: Diel aquatic CO₂ system dynamics of a
1027 Bermudian mangrove environment. *Aquat. Geochem.*, 17(6), 841,
1028 <https://doi.org/10.1007/s10498-011-9142-3>, 2011.
- 1029 Zurbrügg, R., Suter, S., Lehmann, M.F., Wehrli, B., Senn, D.B.: Organic carbon and nitrogen
1030 export from a tropical dam-impacted floodplain system, *Biogeosciences*, 10, 23–38,
1031 [doi:10.5194/bg-10-23-2013](https://doi.org/10.5194/bg-10-23-2013), 2013.
- 1032
- 1033
- 1034



1035



1036

1037 **Fig. 1.** Maps of the study area and of Dhanchi Island, located in the Indian part of the Sundarban
1038 mangroves. The red stars denote the sampling locations within the two creeks (stations C1 and
1039 C2), the three island boundary stations (IB1, IB2, and IB3) and the three mid-river stations
1040 (MR1, MR2, and MR3), along with the stations for the freshwater end-member (FWEM) and
1041 marine end-member (MEM) sample collections.

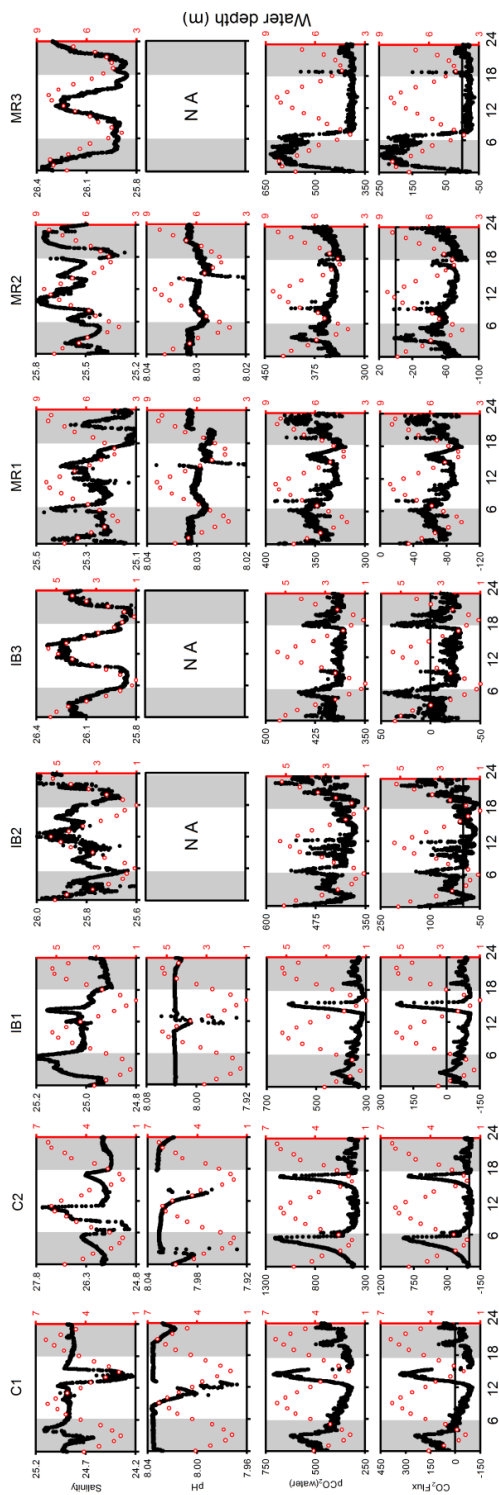
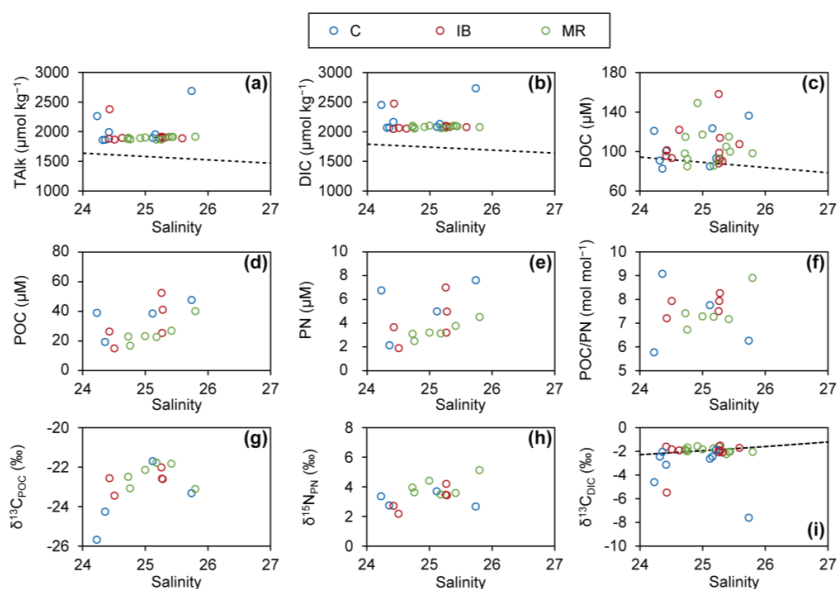


Fig. 2 Time series plots of diel variation (presented in hour) of salinity, pH, $p\text{CO}_2(\text{water})$ (μatm), and CO_2 flux ($\mu\text{mol m}^{-2} \text{h}^{-1}$), at the two creek stations (C1 and C2), the three island boundary stations (IB1, IB2, and IB3) and the three mid-river stations (MR1, MR2, and MR3), along with the variation in water depth (metres, shown on secondary y-axis). NA denotes that data could not be acquired because of unavoidable circumstances. The shaded regions show the night-time of the diel cycle.



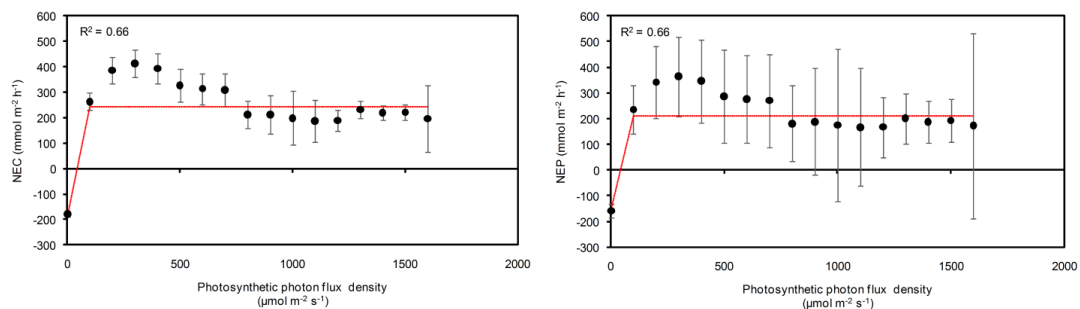
1047

1048 **Fig. 3** Distribution of (a) TAlk, (b) DIC, (c) DOC, (d) POC, (e) PN, (f) POC:PN, (g) $\delta^{15}\text{N}_{\text{PN}}$, (h)
1049 $\delta^{13}\text{C}_{\text{POC}}$, and (i) $\delta^{13}\text{C}$ of DIC, as a function of salinity, at creek (C), island boundary (IB), and
1050 mid-river (MR) stations. The predicted two-end-member conservative mixing distributions of the
1051 respective parameters are shown as dotted lines, assuming the following measured values for the
1052 freshwater end-member (FWEM) and the marine end-member (MEM): FWEM TAlk = 2977 μM
1053 kg^{-1} , MEM TAlk = 1646 μM kg^{-1} ; FWEM DIC = 2950 μM kg^{-1} , MEM DIC = 1476 μM kg^{-1} ;
1054 FWEM DOC = 218.0 μM , MEM DOC = 79.2 μM ; FWEM $\delta^{13}\text{C}_{\text{DIC}} = -6.6\text{‰}$, MEM $\delta^{13}\text{C}$ of DIC
1055 = -1.2‰ .

1056

1057

1058



1059

1060 **Fig. 4** Bin average net ecosystem calcification (NEC) and net ecosystem production (NEP)
1061 values at C2 plotted against photosynthetic photon flux density. The red lines show the
1062 photosynthesis–irradiance curve fitted to measured NEP and NEC, and is statistically significant
1063 ($P < 0.0001$). The R^2 values are displayed on the respective plots. Error bars indicates standard
1064 deviation.

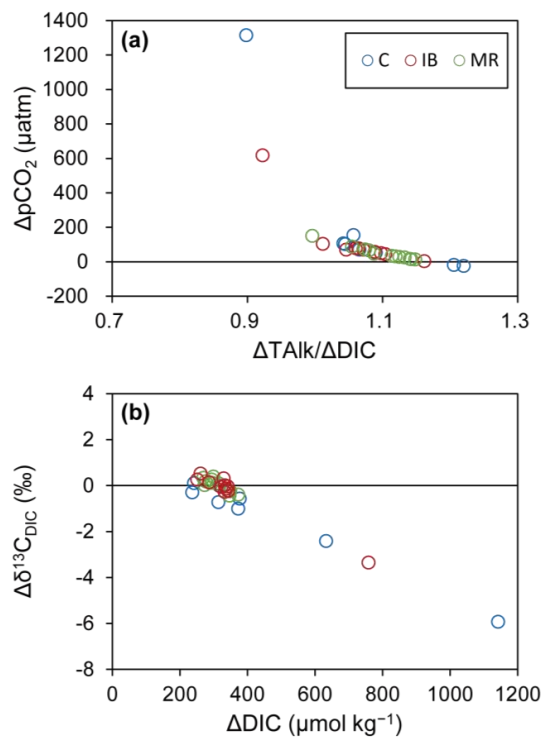
1065

1066

1067

1068

1069



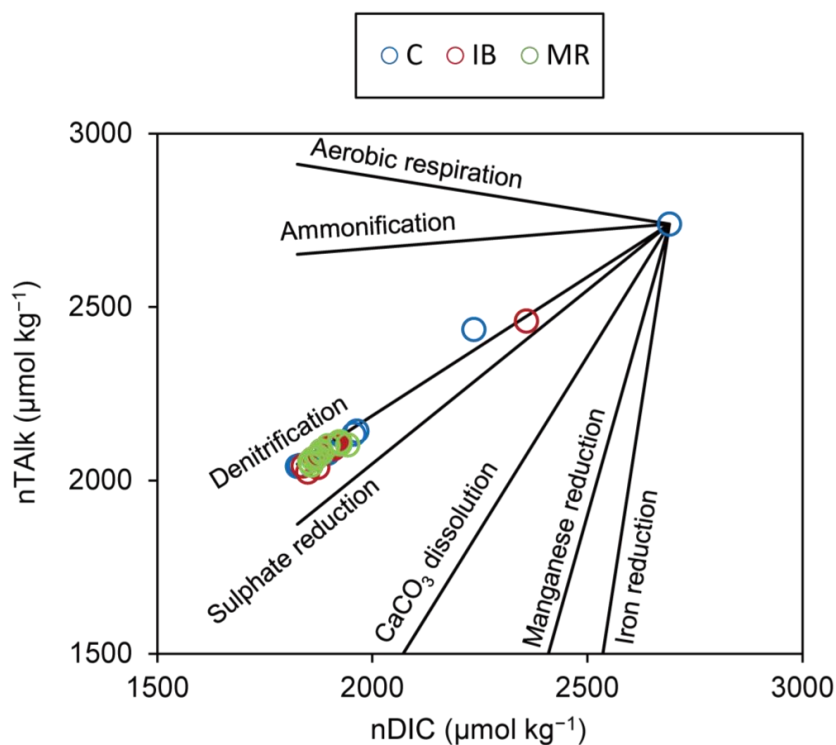
1070

1071

1072 **Fig. 5. (a)** Relationship between the $\Delta TAlk:\Delta DIC$ ratio and ΔpCO_2 [the difference between the
1073 in situ value of pCO_2 (water) estimated using measured TAlk and DIC and the conservative
1074 mixing value for the same]. **(b)** Deviation plot (ΔDIC vs. $\Delta \delta^{13}C_{DIC}$).

1075

1076



1077

1078 **Fig. 6.** Salinity-normalized TALK (nTALK) vs. salinity-normalized DIC (nDIC). The lines
1079 correspond to the theoretical covariation of nTALK and nDIC for various metabolic pathways,
1080 and the coloured circles indicate data from the present study.

1081

1082

1083

1084

1085



1086

1087 **Table 1** pCO₂(water) and air–water CO₂ flux observed in this study, and from the most recent
 1088 studies that measured pCO₂(water) and/or air–water CO₂ flux directly from the mangroves
 1089 surrounding waters.

Place	pCO ₂ (water) [μatm]	CO ₂ flux (mmol CO ₂ m ⁻² d ⁻¹)	Remarks	Authors
North Brazil	592 to 15,361	174 ± 129	Spring to neap tidal cycle	Call et al. (2019)
Ouemo archipelago, New Caledonia	NA	11 to 1620	Dec, 2016 to Sept, 2017 (three week interval) only during high tide sessions	Jacotot et al. (2018)
Vietnam	660 to 5000	74 to 876	24 h cycle in dry and wet season	David et al. (2018)
Queensland, Australia	387 to 13031	58.7 to 277.6	Wet season and dry season	Rosentreter et al. (2018)
Bali, Indonesia	NA	18.1 ± 5.8	55 h time series measurement	Macklin et al. (2019)
Iriomote Island, Japan	394 to 2667	9.1 ± 11.3	July, 2017	unpublished data, Akhand et al.
Sundarban, India	311 to 1204	-0.7 ± 1.7 to 1.6 ± 4.3	Two weeks of post-monsoon (dry) season	Present study

1090